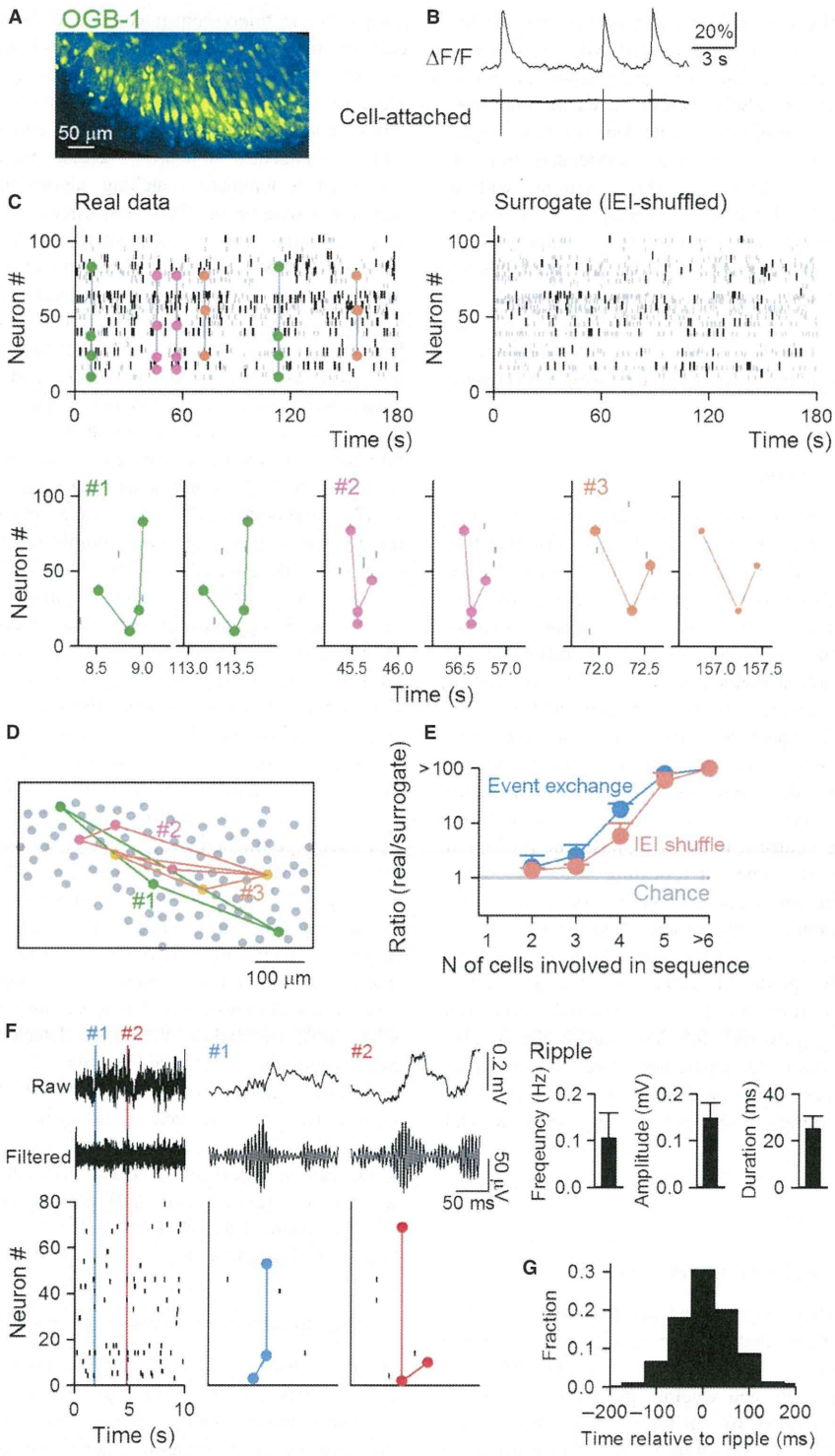

FIG. 1. Statistical salience of repeating sequences in ongoing network activity. (A) Confocal image of a hippocampal slice loaded with OGB-1. (B) Simultaneous recordings of somatic calcium signals sampled at a frame rate of 50 Hz (top) and juxtacellular currents (bottom) from the same neuron indicate that calcium transients reflect the firing of action potentials. (C) A sample rastergram showing repeating sequences. Each dot represents a single calcium event. Events involved and not involved in sequences are shown as black and gray dots, respectively. Three representative repeating sequences are shown as connected lines and magnified in time in the three bottom panels. The right panel shows a surrogate rastergram generated by the IEI-shuffling procedure. (D) The locations of the cells in the sequences shown in (C). (E) The average ratios of the number of sequences in real datasets to those in 20 surrogate datasets (n = 5 slices) are plotted as a function of the number of neurons involved in sequences. (F) Simultaneous recordings of CA3 local field potentials band-pass filtered at 150–250 Hz (top) and activity patterns of the neuronal population (bottom). Two representative ripple events are magnified in the right insets, depicting sequence emergence corresponding with the timing of ripple generation. Right bar graphs show the basic properties of ripples (n = 154 ripples from five slices). (G) Cross-correlogram of repeating sequences with CA3 ripple events (n = 108).

with a 1% false-positive error rate (Sasaki *et al.*, 2009). As shown in Fig. 2A, we first monitored ongoing network activity under conditions of (in mM): K^+, 4.2; Mg^{2+}, 1.5; Ca^{2+}, 1.5, for 10 min to detect relay sequences. We then changed the extracellular solution to the modified aCSF (in mM: K^+, 2.2; Mg^{2+}, 3.0; Ca^{2+}, 3.2). This procedure was employed to minimize spontaneous activity and synaptic transmission failure, and thereby increase the fidelity of ROTing. After the network stabilization, we clamped two-five neurons at a holding potential of 0 mV to record inhibitory PSCs, and monitored the spatiotemporal firing patterns of neurons using fMCI (Fig. 2B). To improve detection accuracy, we conducted whole-cell recordings from two-five neurons that were located at an inter-cell distance of > 50 μm. A cocktail of ionotropic glutamate receptor antagonists, CNQX and AP5, was applied so that PSCs reflected inhibitory activities more faithfully. Under these conditions, we applied 50 mM K^+ through a glass pipette and induced calcium events in a small fraction of neurons. The pipette was slowly moved over the pyramidal cell layer to equally activate as many neurons as possible (Fig. 2C). Some calcium events in different neurons coincided during relatively short time periods, but most of them were not fully synchronized and were separable. We analysed the relative timing between calcium events of individual neurons and inhibitory PSCs of the patched neurons, and determined putative inhibitory neurons that projected to the patch-clamped neuron. In the example data shown in Fig. 2D, the timings of the calcium events of neuron #37 coincided significantly with the timings of PSCs, with a *P*-value < 0.01, which indicates that this neuron could be a presynaptic cell candidate that transmits inhibitory transmission to the patched neuron. By applying this analysis to all imaged neurons, we defined the positions of putative inhibitory cells. The ratio of putative inhibitory neurons to total active neurons was 19.1 ± 1.8% (n = 295 active cells from five slices). This fraction is in agreement with the estimation that the overall proportion of interneurons in the hippocampal pyramidal cell layer is ~20% (Freund & Buzsaki, 1996). Based on the offline identification of putative excitatory and inhibitory cells, we separately reconstructed their ongoing activity patterns (Fig. 2F) that were recorded before application of ROTing (for procedure, see Fig. 2A). The frequency of spontaneous activity of inhibitory neurons was slightly higher than that of excitatory neurons, but the difference was not statistically significant (Fig. 2G).

Inhibitory neurons are active before repeating sequences

We then investigated how excitatory and inhibitory neurons are engaged in the sequential events. The ratios of the number of events participating in sequences to the total number of events were 41.8 ± 3.9% and 35.8 ± 8.8% in excitatory (n = 515 cells) and inhibitory (n = 54 cells) cells, respectively. To examine the activity changes before and after the appearance of repeating sequences, we aligned rastergrams of population activity to the onset of individual sequences (Fig. 3A). The resulting peri-event time histogram revealed that the firing rates of inhibitory cells increased progressively before the emergence of repeating sequences; the mean calcium event frequency of inhibitory cells increased significantly by 510% during a period of 20–100 ms before the onset of repeating sequences (Fig. 3B; P = 0.031, t_4 = 3.24, paired-t test, n = 54 cells from five slices). In contrast, no elevation of the firing rate occurred in excitatory cells (P > 0.05, n = 515 cells). Once sequences started, excitatory and inhibitory neurons showed 3.4 and 4.5 times increases in their firing rates, respectively (P < 0.05, Tukey's test after ANOVA). These firing rate changes resembled those observed during SW-Rs (Csicsvari *et al.*, 1999, 2000; Klausberger *et al.*, 2003).

We analysed the activity patterns of individual inhibitory cells and identified interneurons that were specifically activated before individual sequences (Fig. 3C). We observed that the same inhibitory neurons tended to be activated prior to the emergence of identical sequences (Fig. 3D). The probability that a sequence was repeatedly preceded by the same inhibitory cell was significantly higher than the probability that a sequence was preceded by different inhibitory cells (Fig. 3D; P = 0.042, t_4 = 2.95, paired t-test). To examine the spatial relationship of the pre-activated interneurons and the subsequent relay sequences, we measured the cell-to-cell distance between the neuron activated first in a sequence and the interneuron that fired ahead of the sequence (Fig. 3E). The mean distance was 61.3 ± 2.4 μm, which was significantly smaller than that obtained from 100 surrogate datasets (Fig. 3F; $P = 1.3 \times 10^{-8}$, D_{1385} = 0.20, Kolmogorov–Smirnov test). The surrogates were generated by random shuffling of the cell identity within each cell map. These results suggest that the generation of repeated sequences was determined by the firing of specific interneurons that were located close to the initiation sites of the sequences.

To further verify the relevance of the selective increase in firing rates in inhibitory cells, we determined if the activity patterns of individual cells can predict the sequence-onset times. In each cell type, we created a vector (prediction vector) that represented the ratios of the number of calcium events that preceded any sequences by 0–100 ms to the number of total events in individual cells (Fig. 4A). The ratio represents the prediction probability that one sequence emerges 0–100 ms after the calcium event of each neuron. Typically, inhibitory cells showed higher probabilities than excitatory cells. Then, the likelihood of the emergence of a repeating sequence was calculated at every instantaneous time by defining the prediction scores as the ratio of the number of correctly predicted events to the total number of predicted events. The prediction scores obtained from inhibitory cells were significantly higher than those from excitatory cells and those of inhibitory cells in IEI-shuffled datasets (Fig. 4B; P < 0.05, Tukey's test, n = 5). Thus, compared with excitatory cells, the activity patterns of inhibitory cells provided a better prediction for sequence emergence.

Next, we examined the firing properties of interneurons with a prediction probability of > 0.20 (termed here 'trigger interneurons'). Based on the temporal patterns of calcium events, individual trigger interneurons were classified into three cell types: oscillatory cells (type 1); bursty cells (type 2); and random firing cells (type 3). Oscillatory cells were defined as cells in which the coefficient of variation of IEIs was < 0.6. Bursty cells were defined as cells in which 40% of the IEIs were < 1 s. Random firing cells were defined as cells that were not classified into the above two types. Out of 20 trigger interneurons, six cells and 10 cells were found to be oscillatory and bursty cells, respectively (Fig. 4C). This result suggests that both firing types are likely to contribute to the generation of repeating sequences.

Activation of a single interneuron can trigger repeating sequences

In order to clarify the causal influence of interneurons on the emergence of repeating sequences, we tested whether stimulation of an interneuron could trigger repeating sequences in surrounding neurons. An anatomically identified interneuron was whole-cell recorded and spike trains were repeatedly evoked while monitoring population activity by fMCI (Fig. 5B). In five cells out of 10 cells recorded, phasic stimulation (200 pA, 500 ms) at a frequency of 0.1 Hz increased the frequency of repeating sequences by

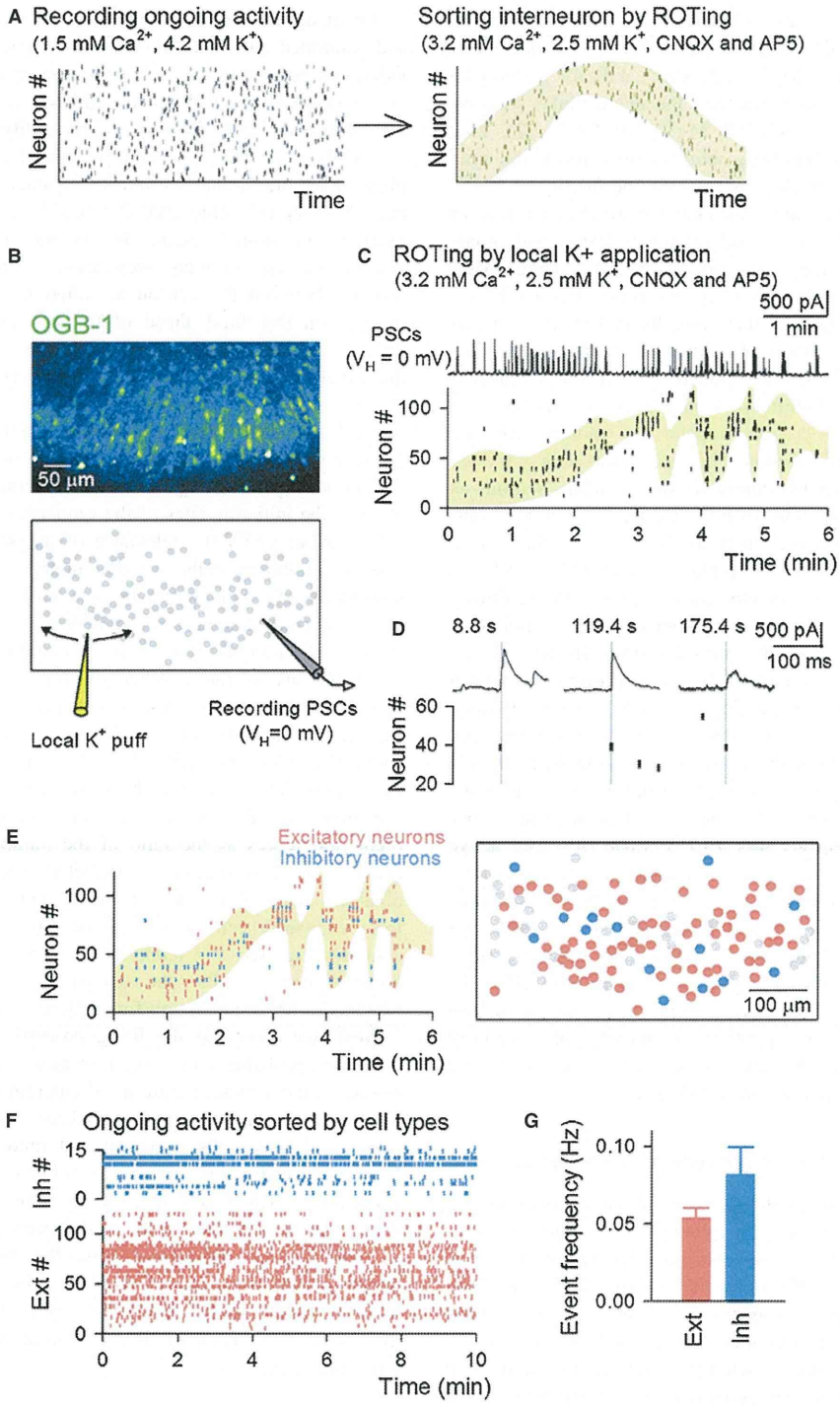

FIG. 2. Mapping of inhibitory neurons in the hippocampal CA3 region. (A) Schematic illustration of the experimental procedure. After recording ongoing activity patterns using fMCI (left), the ionic composition of the aCSF was modified to 3.2 mM Ca^{2+} and 2.2 mM K^+, and ionotropic glutamate receptor antagonists (CNQX and AP5) were added. Then, reverse optical trawling (ROTing) was performed to identify interneurons (right). (B) Confocal image of a hippocampal slice loaded with OGB-1 (top); 125 neurons were searched for inhibitory synaptic connections (bottom). A few neurons were activated by the local application of K^+ through a glass pipette (yellow pipette), which was manually moved over the network. The evoked activity patterns were monitored using fMCI, and inhibitory PSCs were recorded from one-three CA3 pyramidal cells in whole-cell configuration at a holding potential of 0 mV. (C) PSCs in a patched neuron (top) and the spatiotemporal pattern of the calcium events of 125 neurons (bottom) in response to K^+ application. Each dot represents a single calcium event. The shaded area indicates the regions activated during movement of the K^+ pipette. (D) Typical events in (C). In this case, the calcium events of neuron #37 were time-locked to PSC onsets, and thus this neuron was identified as a presynaptic cell candidate that innervated the patched neuron. (E) Calcium events of putative excitatory and inhibitory neurons in the same plot shown in (C) (left). The locations of these cells are shown in the cell map (right). Neurons that did not exhibit activity during ROTing are shown in light gray. (F) A typical rastergram of ongoing calcium events of 110 putative excitatory and 15 inhibitory neurons. (G) The mean frequency of calcium events of 515 excitatory and 54 inhibitory cells. Error bars are SEM.

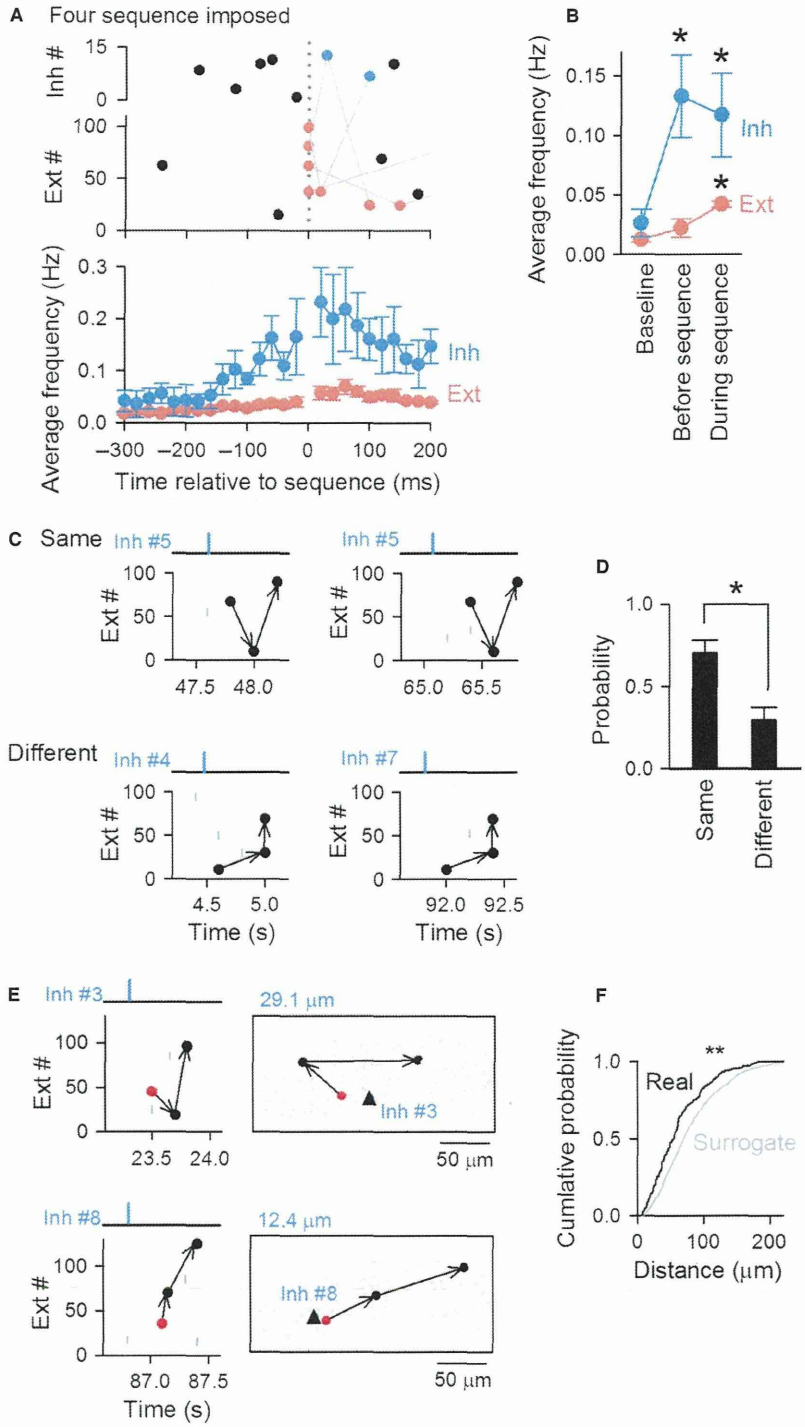

FIG. 3. Sequence-preceding activation of inhibitory neurons. (A) (top) Four representative repeating sequences (gray lines) were aligned to the timing of their first activities in the sequences. Unconnected plots (Smith *et al.*, 2004) represent events not involved in sequences. (Bottom) Peri-event time histogram summarizing the changes in the mean firing rates of 515 excitatory and 54 inhibitory cells relative to the onset of repeating sequences. (B) The average event frequencies at baseline (Baseline), 20–100 ms before each sequence (Before sequence), and during the repeating sequences (During sequence). Error bars are SEM. $*P < 0.05$, Tukey's test after one-way ANOVA. (C) Representative sequences preceded by the same inhibitory cell #5 (top, same), or different cells #4 and #7 (bottom, different). Calcium event onsets of the focused inhibitory cells are shown in blue on the top of the corresponding rastergrams. Neuronal events involved and not involved in sequences are shown in black and gray, respectively, in the rastergrams. Relay sequences are indicated by the arrows. (D) The probabilities that repeating sequences are preceded by the same or different inhibitory cells are compared. Error bars are SEM. $*P < 0.05$, paired *t*-test. (E) Two examples of repeating sequences and the spatial arrangements of the participating neurons. The inhibitory cells activated before the sequences are shown in the triangle. (F) The cumulative probability distribution of the cell-to-cell distances between the first active cells in individual sequences and the inhibitory cells that were activated before the emergence of the sequences is compared with that in 100 surrogates, which were generated by random shuffling of the cell identity in the same cell map. $**P < 0.01$, Kolmogorov–Smirnov test.

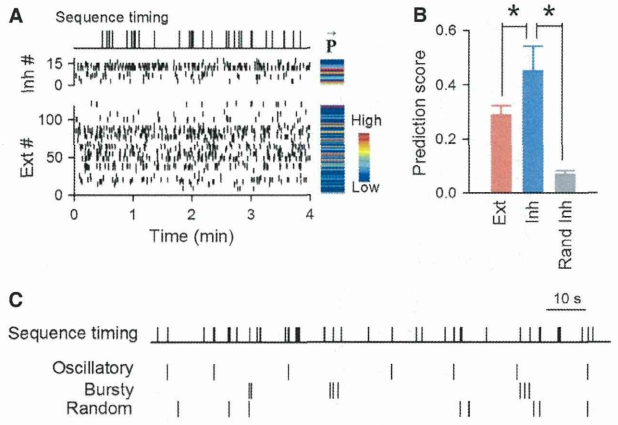

FIG. 4. Prediction of the occurrence of repeating sequences by interneuron firing. (A) The timing of individual repeating sequences (top) was extracted from the rastergram (bottom). Gray-scale images (right) show the prediction vector $P^{\rightarrow}$ for the rastergram, which represents the percentage of the events detected 0–100 ms before sequence emergence in each cell. (B) The mean prediction scores are compared between excitatory and inhibitory cells. The score calculated from IEI-shuffled activity in inhibitory cells is shown in gray. Error bars are SEM. $^*P < 0.05$, Tukey's test after ANOVA. (C) Times of repeating sequences (top) and calcium events of representative oscillatory, bursty and random firing interneurons (bottom).

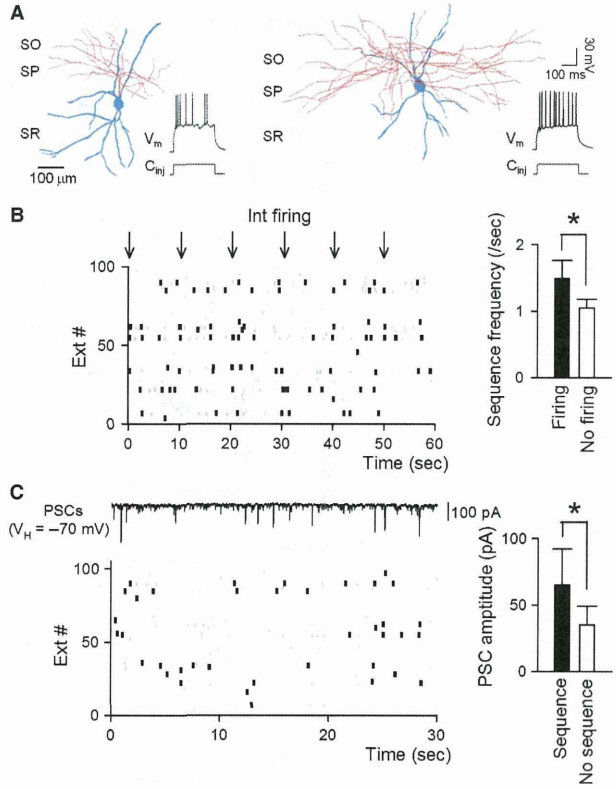

FIG. 5. Stimulation of an interneuron can trigger repeating sequences. (A) Representative reconstruction of two interneurons as visualized with Alexa 568 labeling on a schematic representation of the hippocampus. Only the main dendrites and axon fibers are illustrated. The typical voltage trace in response to a suprathreshold current pulse (200 pA) is shown in the right inset. (B) Simultaneous current injection of the interneuron shown in (A, left) and optical imaging of population activity by fMCI. The frequency of sequences increased in phase with the times of interneuronal firing (arrows). Events involved and not involved in sequences are shown as black and gray dots, respectively. The right panel shows the frequency of sequences with and without the interneuronal firing. Error bars are SEM. $^*P < 0.05$, paired t-test. (C) Simultaneous voltage-clamp recording of an interneuron (top, $V_H = -70$ mV) combined with fMCI (bottom). The right panel shows the amplitude of PSCs 0–500 ms before the emergence of repeating sequences (sequence). The average amplitudes in other periods are shown as 'No sequence'. Error bars are SEM. $^*P < 0.05$, paired t-test.

125–220% within 500 ms after the interneuron firing ($P = 0.038$, $t_4 = 3.06$, paired t-test). These cells that were successful in triggering sequences show fast-spiking or non-fast-spiking responses to current injection (Fig. 5A). Both types possessed multipolar dendrites and exhibited dense preferential innervation of the CA3 principal cell layer, suggesting a perisomatic interneuron subtype (Fig. 5A). Voltage-clamp recordings revealed that these successful neurons received strong PSCs prior to the onset of sequence occurrence (Fig. 5C; $P = 0.039$, $t_4 = 3.03$, paired t-test). These results suggest that a subset of hippocampal interneurons receive strong synaptic inputs that drive their spikes preceding repeating sequences, which in turn determines active cell patterns in the following sequences.

Discussion

Recent advances in multi-channel unit recordings from behaving animals have revealed that distinct subsets of neurons are repeatedly activated during both waking and sleep; this repeated activation could underlie memory consolidation and retrieval (O'Neill *et al.*, 2010; Carr *et al.*, 2011; Schwindel & McNaughton, 2011). In the present work, we took advantage of functional optical imaging and analysed the temporal relationships between the emergence of repeating sequences and individual spikes. We discovered that inhibitory interneurons, rather than excitatory pyramidal cells, exhibited an enhanced activity level before the initiation of repeating sequences. Moreover, we observed that pre-activated interneurons were located in the vicinity of the neurons that were activated first in sequences.

Hippocampal interneurons *in vivo* preferentially discharge action potentials in discrete time windows relative to the timing of SW-Rs, suggesting unique roles in synchronous network oscillations (Ylinen *et al.*, 1995; Klausberger *et al.*, 2003). Parvalbumin-expressing basket cells increase their firing rates during SW-Rs (Lapray *et al.*, 2012). The activation of perisomatic-targeting interneurons is sufficient to trigger SW-Rs by controlling the balance between excitatory and inhibitory inputs in a subpopulation of pyramidal neurons (Ellender *et al.*, 2010). Additionally, the firing of axo-axonic cells, which exclusively target the pyramidal cell axon initial segment, is transiently enhanced at the beginning of SW-Rs and strongly suppressed during SW-Rs (Klausberger *et al.*, 2003; Viney *et al.*, 2013). Taken together, these stereotyped inhibitory cells may collaboratively provide conditions permissive for the initiation of SW-Rs. In addition to this notion, our findings indicate that inhibitory neurons play a crucial role not only in triggering the flow of network oscillations but also in creating precise repeating sequences in hippocampal circuits.

The frequency of ripple oscillations in cultured slices was 0.10 ± 0.05 Hz (Fig. 1F), and lower than those reported in acute slice preparations (≥ 0.5 Hz; Maier *et al.*, 2003; Wu *et al.*, 2005; Norimoto *et al.*, 2012; Hajos *et al.*, 2013). It was rather comparable to the frequency observed in *in vivo* animals, ranging from 0.05 to 0.5 Hz. This might be owing to the recovery of connectivity among neurons in culture. In addition, acute slice preparations require a

high perfusion rate (3–15 mL/min) for metabolic supply to generate SW-Rs, whereas the perfusion rate of 1.5–2.0 mL/min was sufficient to obtain SW-Rs in our cultured slices. Therefore, mechanisms underlying SW-Rs in cultured slices might differ from those in acute slices. To extrapolate our results to *in vivo* brain functions, further experimental work will be required using an advanced experimental approach.

The emergence of repeating sequences has been theoretically predicted by the synfire chain hypothesis (Abeles, 1991), which posits that the precisely timed reactivation of distinct neuronal subsets propagates through neural networks (Diesmann *et al.*, 1999). Such precise firing sequences have been verified in recent decades (Prut *et al.*, 1998; Mao *et al.*, 2001; Ikegaya *et al.*, 2004; Luczak *et al.*, 2007). However, the existence of reactivated patterns with millisecond precision has been called into question by the claim that repeating patterns in spike trains (Baker & Lemon, 2000; Oram *et al.*, 2001) and membrane potential fluctuations (Mokeichev *et al.*, 2007) could occur by chance. This contradiction arises from different assumptions for creating surrogates to be compared with the original datasets. In general, too strong statistical assumptions cause false-negative detection of sequences and tend to lead to a conclusion against the existence of sequences. In fact, neuronal networks are non-randomly woven by synaptic connections (Song *et al.*, 2005; Yoshimura *et al.*, 2005; Yu *et al.*, 2009). Because in the biological system the function is tightly coupled to the structure, it is a natural consequence that functional activities emitted by a non-randomly structured neuronal network are non-randomly patterned in space and time. We thus suspect that the failure to reject the null hypothesis against the sequence existence in several studies is simply due to inappropriate statistical assumptions for data surrogates.

The contributions of inhibitory circuits to the regulation of repeating sequences are attributable to a variety of physiological principles at the single-cell level. One of the most likely mechanisms is that inhibitory inputs reset the regular firing of principal cells that are not originally a part of the sequence, and delay their firing to enable their participation in a later phase of the sequence. On a millisecond time scale, feed forward interneurons preserve the temporal fidelity of synaptic integration and action potential generation in pyramidal cells (Pouille & Scanziani, 2001; Lamsa *et al.*, 2005). In addition to such inhibitory effects, interneurons can elicit a post-inhibitory rebound depolarization, which in turn is capable of triggering an action potential or a short burst of spikes within a restricted time window (Lytton & Sejnowski, 1991; Buzsaki & Chrobak, 1995; Cobb *et al.*, 1995; Ellender *et al.*, 2010). Assuming that numerous pyramidal cells share the common subthreshold influence of a single presynaptic interneuron (Freund & Buzsaki, 1996; Fino & Yuste, 2011), the synergistic effects of phase resetting and depolarizing overshoot could powerfully regulate the dynamics of neuronal ensembles. In line with this prediction, a recent paper has demonstrated that the activation of single inhibitory neurons can more effectively induce synchronous activity patterns in the developing hippocampus (Bonifazi *et al.*, 2009) and animal behavioral responses (Houweling & Brecht, 2008) than the activation of excitatory principal cells. Taken together, we suggest that inhibitory interneurons perform the dynamic selection and control of precisely timed replay in neuronal ensembles, leading to information transfer, memory formation and retrieval in the cortex.

Acknowledgements

This work was partly supported by Grants-in-Aid for Science Research on Innovative Areas, 'Mesoscopic Neurocircuitry' (no. 22115003), from the Ministry of Education, Culture, Sports, Science and Technology of Japan, and by the Funding Program for Next Generation World-Leading Researchers (LS023).

Abbreviations

aCSF, artificial cerebrospinal fluid; AP5, D,L-2-amino-5-phosphonopentanoic acid; CNQX, 6-cyano-7-nitroquinoxaline-2,3-dione; fMCI, functional multineuron calcium imaging; IEI, inter-event interval; OGB-1, Oregon Green 488 BAPTA-1; PSC, postsynaptic current; ROTing, reverse optical trawling; SW-R, sharp wave and ripple.

References

Aaron, G. & Yuste, R. (2006) Reverse optical probing (ROPING) of neocortical circuits. *Synapse*, **60**, 437–440.
Abeles, M. (1991) *Corticonics: Neural Circuits of the Cerebral Cortex*. Cambridge University Press, Cambridge, MA.
Baker, S.N. & Lemon, R.N. (2000) Precise spatiotemporal repeating patterns in monkey primary and supplementary motor areas occur at chance levels. *J. Neurophysiol.*, **84**, 1770–1780.
Bandyopadhyay, S., Shamma, S.A. & Kanold, P.O. (2010) Dichotomy of functional organization in the mouse auditory cortex. *Nat. Neurosci.*, **13**, 361–368.
Bonifazi, P., Goldin, M., Picardo, M.A., Jorquera, I., Cattani, A., Bianconi, G., Represa, A., Ben-Ari, Y. & Cossart, R. (2009) GABAergic hub neurons orchestrate synchrony in developing hippocampal networks. *Science*, **326**, 1419–1424.
Busche, M.A., Eichhoff, G., Adelsberger, H., Abramowski, D., Wiederhold, K.H., Haass, C., Staufenbiel, M., Konnerth, A. & Garaschuk, O. (2008) Clusters of hyperactive neurons near amyloid plaques in a mouse model of Alzheimer's disease. *Science*, **321**, 1686–1689.
Buzsaki, G. & Chrobak, J.J. (1995) Temporal structure in spatially organized neuronal ensembles: a role for interneuronal networks. *Curr. Opin. Neurobiol.*, **5**, 504–510.
Carr, M.F., Jadhav, S.P. & Frank, L.M. (2011) Hippocampal replay in the awake state: a potential substrate for memory consolidation and retrieval. *Nat. Neurosci.*, **14**, 147–153.
Cobb, S.R., Buhl, E.H., Halasy, K., Paulsen, O. & Somogyi, P. (1995) Synchronization of neuronal activity in hippocampus by individual GABAergic interneurons. *Nature*, **378**, 75–78.
Csicsvari, J., Hirase, H., Czurko, A., Mamiya, A. & Buzsaki, G. (1999) Oscillatory coupling of hippocampal pyramidal cells and interneurons in the behaving Rat. *J. Neurosci.*, **19**, 274–287.
Csicsvari, J., Hirase, H., Mamiya, A. & Buzsaki, G. (2000) Ensemble patterns of hippocampal CA3-CA1 neurons during sharp wave-associated population events. *Neuron*, **28**, 585–594.
Diba, K. & Buzsaki, G. (2007) Forward and reverse hippocampal place-cell sequences during ripples. *Nat. Neurosci.*, **10**, 1241–1242.
Diesmann, M., Gewaltig, M.O. & Aertsen, A. (1999) Stable propagation of synchronous spiking in cortical neural networks. *Nature*, **402**, 529–533.
Dragoi, G. & Tonegawa, S. (2011) Preplay of future place cell sequences by hippocampal cellular assemblies. *Nature*, **469**, 397–401.
Ellender, T.J., Nissen, W., Colgin, L.L., Mann, E.O. & Paulsen, O. (2010) Priming of hippocampal population bursts by individual perisomatic-targeting interneurons. *J. Neurosci.*, **30**, 5979–5991.
Fino, E. & Yuste, R. (2011) Dense inhibitory connectivity in neocortex. *Neuron*, **69**, 1188–1203.
Foster, D.J. & Wilson, M.A. (2006) Reverse replay of behavioural sequences in hippocampal place cells during the awake state. *Nature*, **440**, 680–683.
Freund, T.F. & Buzsaki, G. (1996) Interneurons of the hippocampus. *Hippocampus*, **6**, 347–470.
Hajos, N., Karlocai, M.R., Nemeth, B., Ulbert, I., Monyer, H., Szabo, G., Erdelyi, F., Freund, T.F. & Gulyas, A.I. (2013) Input-output features of anatomically identified CA3 neurons during hippocampal sharp wave/ripple oscillation *in vitro*. *J. Neurosci.*, **33**, 11677–11691.
Houweling, A.R. & Brecht, M. (2008) Behavioural report of single neuron stimulation in somatosensory cortex. *Nature*, **451**, 65–68.
Ikegaya, Y., Aaron, G., Cossart, R., Aronov, D., Lampl, I., Ferster, D. & Yuste, R. (2004) Synfire chains and cortical songs: temporal modules of cortical activity. *Science*, **304**, 559–564.
Karlsson, M.P. & Frank, L.M. (2009) Awake replay of remote experiences in the hippocampus. *Nat. Neurosci.*, **12**, 913–918.

Klausberger, T., Magill, P.J., Marton, L.F., Roberts, J.D., Cobden, P.M., Buzsaki, G. & Somogyi, P. (2003) Brain-state- and cell-type-specific firing of hippocampal interneurons *in vivo*. *Nature*, **421**, 844–848.

Komiyama, T., Sato, T.R., O'Connor, D.H., Zhang, Y.X., Huber, D., Hooks, B.M., Gabitto, M. & Svoboda, K. (2010) Learning-related fine-scale specificity imaged in motor cortex circuits of behaving mice. *Nature*, **464**, 1182–1186.

Koyama, R., Muramatsu, R., Sasaki, T., Kimura, R., Ueyama, C., Tamura, M., Tamura, N., Ichikawa, J., Takahashi, N., Usami, A., Yamada, M.K., Matsuki, N. & Ikegaya, Y. (2007) A low-cost method for brain slice cultures. *J. Pharmacol. Sci.*, **104**, 191–194.

Lamsa, K., Heeroma, J.H. & Kullmann, D.M. (2005) Hebbian LTP in feed-forward inhibitory interneurons and the temporal fidelity of input discrimination. *Nat. Neurosci.*, **8**, 916–924.

Lapray, D., Lasztoczi, B., Lagler, M., Viney, T.J., Katona, L., Valenti, O., Hartwich, K., Borhegyi, Z., Somogyi, P. & Klausberger, T. (2012) Behavior-dependent specialization of identified hippocampal interneurons. *Nat. Neurosci.*, **15**, 1265–1271.

Luczak, A., Bartho, P., Marguet, S.L., Buzsaki, G. & Harris, K.D. (2007) Sequential structure of neocortical spontaneous activity *in vivo*. *Proc. Natl. Acad. Sci. USA*, **104**, 347–352.

Lytton, W.W. & Sejnowski, T.J. (1991) Simulations of cortical pyramidal neurons synchronized by inhibitory interneurons. *J. Neurophysiol.*, **66**, 1059–1079.

MacLean, J.N., Watson, B.O., Aaron, G.B. & Yuste, R. (2005) Internal dynamics determine the cortical response to thalamic stimulation. *Neuron*, **48**, 811–823.

Maier, N., Nimmrich, V. & Draguhn, A. (2003) Cellular and network mechanisms underlying spontaneous sharp wave-ripple complexes in mouse hippocampal slices. *J. Physiol.*, **550**, 873–887.

Mao, B.Q., Hamzei-Sichani, F., Aronov, D., Froemke, R.C. & Yuste, R. (2001) Dynamics of spontaneous activity in neocortical slices. *Neuron*, **32**, 883–898.

Margolis, D.J., Lutcke, H., Schulz, K., Haiss, F., Weber, B., Kugler, S., Hasan, M.T. & Helmchen, F. (2012) Reorganization of cortical population activity imaged throughout long-term sensory deprivation. *Nat. Neurosci.*, **15**, 1539–1546.

Matsumoto, K., Ishikawa, T., Matsuki, N. & Ikegaya, Y. (2013) Multineuronal spike sequences repeat with millisecond precision. *Front. Neural. Circuits*, **7**, 112.

Mokeichev, A., Okun, M., Barak, O., Katz, Y., Ben-Shahar, O. & Lampl, I. (2007) Stochastic emergence of repeating cortical motifs in spontaneous membrane potential fluctuations *in vivo*. *Neuron*, **53**, 413–425.

Norimoto, H., Mizunuma, M., Ishikawa, D., Matsuki, N. & Ikegaya, Y. (2012) Muscarinic receptor activation disrupts hippocampal sharp wave-ripples. *Brain Res.*, **1461**, 1–9.

Ohki, K., Chung, S., Kara, P., Hubener, M., Bonhoeffer, T. & Reid, R.C. (2006) Highly ordered arrangement of single neurons in orientation pinwheels. *Nature*, **442**, 925–928.

O'Neill, J., Pleydell-Bouverie, B., Dupret, D. & Csicsvari, J. (2010) Play it again: reactivation of waking experience and memory. *Trends Neurosci.*, **33**, 220–229.

Oram, M.W., Hatsopoulos, N.G., Richmond, B.J. & Donoghue, J.P. (2001) Excess synchrony in motor cortical neurons provides redundant direction information with that from coarse temporal measures. *J. Neurophysiol.*, **86**, 1700–1716.

Pouille, F. & Scanziani, M. (2001) Enforcement of temporal fidelity in pyramidal cells by somatic feed-forward inhibition. *Science*, **293**, 1159–1163.

Prut, Y., Vaadia, E., Bergman, H., Haalman, I., Slovin, H. & Abeles, M. (1998) Spatiotemporal structure of cortical activity: properties and behavioral relevance. *J. Neurophysiol.*, **79**, 2857–2874.

Sasaki, T., Matsuki, N. & Ikegaya, Y. (2007) Metastability of active CA3 networks. *J. Neurosci.*, **27**, 517–528.

Sasaki, T., Takahashi, N., Matsuki, N. & Ikegaya, Y. (2008) Fast and accurate detection of action potentials from somatic calcium fluctuations. *J. Neurophysiol.*, **100**, 1668–1676.

Sasaki, T., Minamisawa, G., Takahashi, N., Matsuki, N. & Ikegaya, Y. (2009) Reverse optical trawling for synaptic connections *in situ*. *J. Neurophysiol.*, **102**, 636–643.

Schwindel, C.D. & McNaughton, B.L. (2011) Hippocampal-cortical interactions and the dynamics of memory trace reactivation. *Prog. Brain Res.*, **193**, 163–177.

Smith, A.C., Frank, L.M., Wirth, S., Yanike, M., Hu, D., Kubota, Y., Graybiel, A.M., Suzuki, W.A. & Brown, E.N. (2004) Dynamic analysis of learning in behavioral experiments. *J. Neurosci.*, **24**, 447–461.

Song, S., Sjostrom, P.J., Reigl, M., Nelson, S. & Chklovskii, D.B. (2005) Highly nonrandom features of synaptic connectivity in local cortical circuits. *PLoS Biol.*, **3**, e68.

Takahashi, N., Sasaki, T., Usami, A., Matsuki, N. & Ikegaya, Y. (2007) Watching neuronal circuit dynamics through functional multineuron calcium imaging (fMCI). *Neurosci. Res.*, **58**, 219–225.

Takahashi, N., Sasaki, T., Matsumoto, W., Matsuki, N. & Ikegaya, Y. (2010) Circuit topology for synchronizing neurons in spontaneously active networks. *Proc. Natl. Acad. Sci. USA*, **107**, 10244–10249.

Takahashi, N., Oba, S., Yukinawa, N., Ujita, S., Mizunuma, M., Matsuki, N., Ishii, S. & Ikegaya, Y. (2011) High-speed multineuron calcium imaging using Nipkow-type confocal microscopy. *Curr. Protoc. Neurosci.*, **2**, 2.14.

Viney, T.J., Lasztoczi, B., Katona, L., Crump, M.G., Tukker, J.J., Klausberger, T. & Somogyi, P. (2013) Network state-dependent inhibition of identified hippocampal CA3 axo-axonic cells *in vivo*. *Nat. Neurosci.*, **16**, 1802–1811.

Wu, C., Asl, M.N., Gillis, J., Skinner, F.K. & Zhang, L. (2005) An *in vitro* model of hippocampal sharp waves: regional initiation and intracellular correlates. *J. Neurophysiol.*, **94**, 741–753.

Ylinen, A., Bragin, A., Nadasdy, Z., Jando, G., Szabo, I., Sik, A. & Buzsaki, G. (1995) Sharp wave-associated high-frequency oscillation (200 Hz) in the intact hippocampus: network and intracellular mechanisms. *J. Neurosci.*, **15**, 30–46.

Yoshimura, Y., Dantzker, J.L. & Callaway, E.M. (2005) Excitatory cortical neurons form fine-scale functional networks. *Nature*, **433**, 868–873.

Yu, Y.C., Bultje, R.S., Wang, X. & Shi, S.H. (2009) Specific synapses develop preferentially among sister excitatory neurons in the neocortex. *Nature*, **458**, 501–504.

Ziv, Y., Burns, L.D., Cocker, E.D., Hamel, E.O., Ghosh, K.K., Kitch, L.J., Gamal, A.E. & Schnitzer, M.J. (2013) Long-term dynamics of CA1 hippocampal place codes. *Nat. Neurosci.*, **16**, 264–266.

Journal of Pharmacological Sciences xxx (2014) 1–5

HOSTED BY

ELSEVIER

Contents lists available at ScienceDirect

Journal of Pharmacological Sciences

journal homepage: www.elsevier.com/locate/jphs

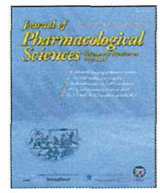

Short communication

Paroxetine prevented the down-regulation of astrocytic L-Glu transporters in neuroinflammation

Koki Fujimori [a, b], Junpei Takaki [a, b], Yukari Shigemoto-Mogami [a], Yuko Sekino [a], Takeshi Suzuki [b], Kaoru Sato [a, *]

[a] Laboratory of Neuropharmacology, Division of Pharmacology, National Institute of Health Sciences, 1-18-1 Kamiyoga, Setagaya-ku, Tokyo 158-8501, Japan
[b] Division of Basic Biological Science, Faculty of Pharmacy, Keio University, 1-5-30 Shiba-koen, Minato-ku, Tokyo 105-8512, Japan

ARTICLE INFO

Article history:
Received 4 August 2014
Received in revised form
26 August 2014
Accepted 18 September 2014
Available online xxx

Keywords:
Paroxetine
L-glutamate
Inflammation

ABSTRACT

The extracellular L-glutamate (L-Glu) concentration is elevated in neuroinflammation, thereby causing excitotoxicity. One of the mechanisms is down-regulation of astrocyte L-Glu transporters. Some antidepressants have anti-inflammatory effects. We therefore investigated effects of various antidepressants on the down-regulation of astrocyte L-Glu transporters in the in vitro neuroinflammation model. Among these antidepressants, only paroxetine was effective. We previously demonstrated that the down-regulation of astrocyte L-Glu transporters was caused by L-Glu released from activated microglia. We here clarified that only paroxetine inhibited L-Glu release from microglia. This is the novel action of paroxetine, which may bring advantages on the therapy of neuroinflammation.

Increasing evidence indicates that inflammatory processes play important roles in the pathogenesis of many neurodegenerative disorders (1–3). Under the neuroinflammatory conditions, it is known that the extracellular concentration of L-glutamate (L-Glu) and inflammatory mediators, such as proinflammatory cytokines, prostaglandins, free radicals and complements are elevated (4). L-Glu is one of the most abundant excitatory neurotransmitters in the mammalian CNS. The released L-Glu is immediately uptaken by astrocyte L-Glu transporters, GLAST (EAAT1 in human) and GLT-1 (EAAT2 in human), or sustained elevation of extracellular concentration of L-Glu induce excitotoxicity. The impairment of the astrocyte L-Glu transporters is reported in various neurological disorders including Alzheimer's disease (5), Parkinson's diseases (6) and amyotrophic lateral sclerosis (7). We found that the expression level of L-Glu transporters in astrocytes of astrocyte-microglia-neuron mixed culture was decreased in the *in vitro* model of the early stage of inflammation in the previous study (8). We clarified the interaction between astrocytes and microglia underlie the down-regulation of L-Glu transporters, i.e., activated microglia release L-Glu and the resulting elevation of extracellular L-Glu cause down-regulation of astrocytic L-Glu transporters. Some antidepressants are known to have anti-inflammatory effects (9, 10). In this study, therefore, we investigated the effects of various antidepressants on the decrease in the astrocytic L-Glu transporter function in the early stage of inflammation and the contribution of microglia to the effects.

Astrocyte-microglia-neuron mixed culture and microglia culture were performed according to the methods previously described (8). Antidepressants and serotonin (5-HT) were dissolved in PBS at 100 μM and 10 mM, respectively, and were diluted with culture medium at the time of use. At 8 DIV, the astrocyte-microglia-neuron mixed culture was treated with 10 ng/mL LPS for 72 h. Antidepressants were applied from 1 h before to the end of the LPS-treatment. Then the concentration of the L-Glu remaining in the culture medium 30 min after changing extracellular concentration of L-Glu to 100 μM was measured. The measurement of the extracellular L-Glu concentration in the medium was performed according to the methods previously described (8). Real-Time Quantitative RT-PCR, Western blotting, immunocytochemistry were also performed according to the methods previously

Abbreviations: ATP, adenosine 5′-triphosphate; CNS, central nervous system; DIV, days *in vitro*; GABA, γ-aminobutyric acid; L-glu, L-glutamate; LPS, lipopolysaccharide; PBS, phosphate-buffered saline; $P2X_4$, P2X prinoceptor 4; RNA, ribonucleic acid; SD, Sprague-Dawley; SDS, sodium dodecyl sulfate; SNRI, serotonin–norepinephrine reuptake inhibitor; SSRI, selective serotonin reuptake inhibitor; TCA, tricyclic antidepressant; 5-HT, 5-hydroxytryptamine.

* Corresponding author. Tel./fax: +81 3 3700 9698.
E-mail address: kasato@nihs.go.jp (K. Sato).

Peer review under responsibility of Japanese Pharmacological Society.

http://dx.doi.org/10.1016/j.jphs.2014.09.002

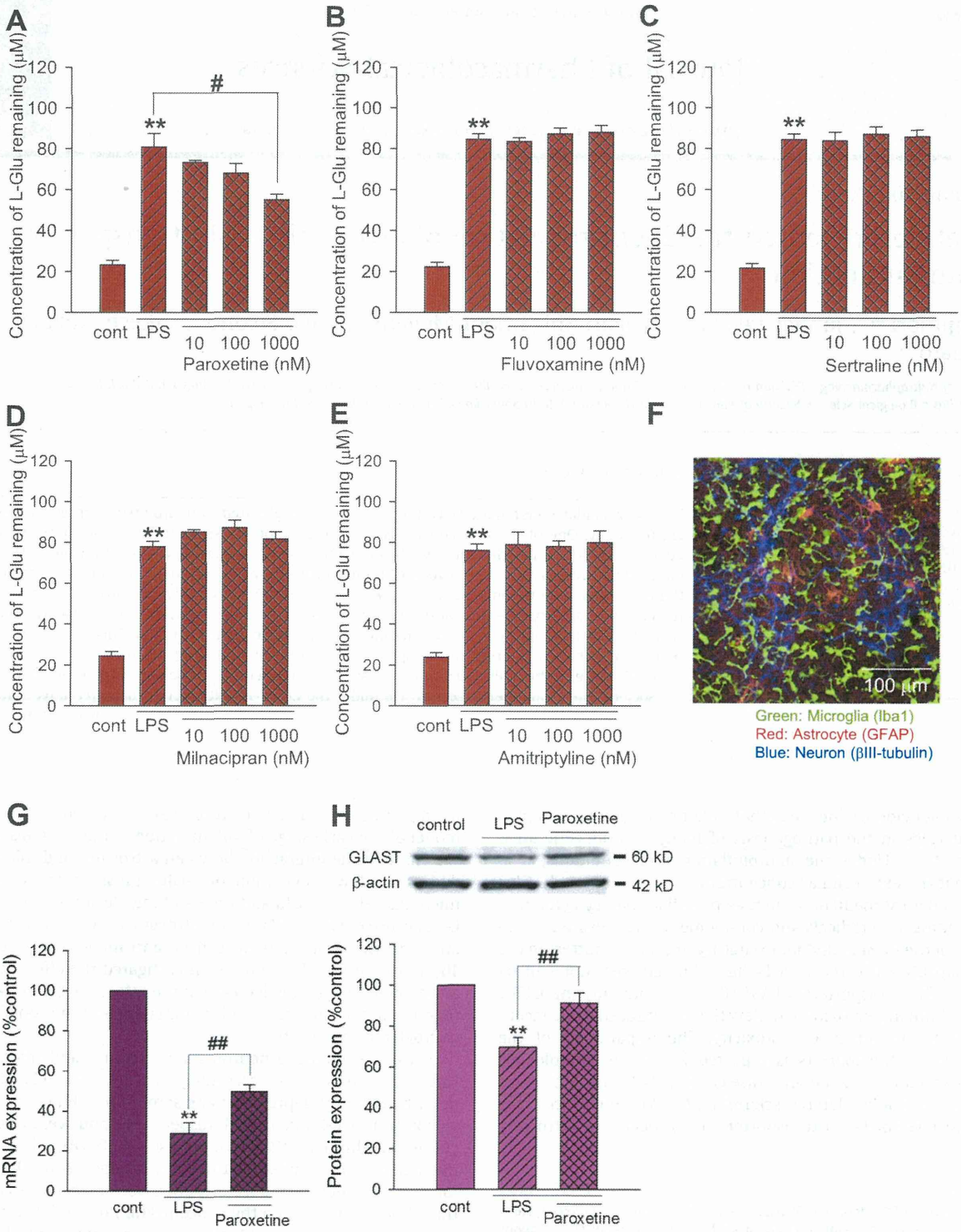

Fig. 1. Effects of antidepressants on the decreased L-Glu transport activity under the inflammatory condition. A–E. Antidepressants were applied to the mixed culture from 1 h before to the end of the LPS-treatment (10 ng/ml, 72 h). L-Glu transport activity was quantified as the L-Glu remaining 30 min after changing the extracellular concentration to 100 μM. Paroxetine prevented the LPS-induced decrease in the L-Glu transport activity in a concentration-dependent manner (A). Fluvoxamine (B), sertraline (C), milnacipran (D), and amitriptyline (E) had no effects. **: $p < 0.01$ vs. control group, #: $p < 0.05$ vs. LPS-treated group, Tukey's test following ANOVA ($N = 6$). F. Typical image of the microglia-astrocyte-neuron mixed culture immunostained with cell type-specific markers (Iba1: microglia; GFAP: astrocytes; βIII tubulin: neurons). G, H. Effects of paroxetine on the expression level of GLAST. Mixed cultures were treated with LPS (10 ng/ml) in the absence or presence of the paroxetine for 24 h (for mRNA level quantification) or 72 h (for protein level quantification). The expression level of GLAST was quantified at mRNA level (G) and protein level (H). LPS (10 ng/ml) caused significant decrease in GLAST mRNA level and paroxetine significantly prevented the decrease (G). LPS (10 ng/ml) caused significant decrease in GLAST protein level and paroxetine almost completely prevented the decrease (H). **: $p < 0.01$ vs. control group, ##: $p < 0.01$ vs. LPS-treated group, Tukey's test following ANOVA ($N = 5$).

Please cite this article in press as: Fujimori K, et al., Paroxetine prevented the down-regulation of astrocytic L-Glu transporters in neuroinflammation, Journal of Pharmacological Sciences (2014), http://dx.doi.org/10.1016/j.jphs.2014.09.002

described (8). The microglia culture was treated with LPS for 24 h in the presence or absence of antidepressants and the concentration of L-Glu in the medium was measured. All sets of the experiments were repeated in triplicate. All procedures described above were in accordance with institutional guidelines.

In the previous report, we showed that the expression level of astrocytic L-Glu transporters was decreased in the astrocyte-microglia-neuron mixed culture in LPS (10 ng/ml, 72 h)-induced inflammation model without cell death (8). We first compared the effects of various groups of antidepressants, i.e., selective serotonin reuptake inhibitors (SSRIs) (paroxetine, fluvoxamine, and sertraline), serotonin–norepinephrine reuptake inhibitor (SNRI) (milnacipran), and tricyclic antidepressant (TCA) (amitriptyline), on the decrease in the astrocytic L-Glu transporter function in this inflammation model. To quantify L-Glu transport activity, we measured the concentration of L-Glu remaining 30 min after changing the medium to the one containing 100 μM of L-Glu. In each set of experiment, LPS-induced decrease in the L-Glu transport activity was stably reproduced (Fig. 1A–E). Among antidepressants, only paroxetine prevented the LPS-induced decrease in L-Glu transport activity (Fig. 1A). The effect was concentration-dependent and reached significant at 1 μM. The other antidepressants had no effects (Fig. 1B–E). Typical image of the astrocyte-microglia-neuron mixed culture was shown in Fig. 1F. We have clarified that LPS-induced decrease in L-Glu transport activity was caused by the decrease in the expression level of GLAST, a predominant L-Glu transporter in the mixed culture, in both of mRNA and protein levels (8). In this study, LPS-induced decreases in the expression of GLAST, were reproduced at both of mRNA (28.8 ± 4.7% of the control) and protein (69.5 ± 4.7% of the control) levels (Fig. 1G, H). We then examined the effects of paroxetine on the LPS-induced decrease in the L-Glu transporter expression. Paroxetine significantly prevented the decreases at both of mRNA (28.8 ± 4.7 to 49.6 ± 3.3%; $n = 10$) and protein (from 69.5 ± 4.7% to 91.0 ± 5.1%; $n = 5$) levels (Fig. 1G, H). As is shown in Fig. 1, fluvoxamine and sertraline, the other SSRIs in this study, did not affect the decrease in L-Glu transport activity, suggesting that paroxetine revealed the effects through the mechanisms independent of its inhibitory effect on serotonin selective transporter. In support of this, LPS-induced decrease in L-Glu transport activity was not changed by the elevation of extracellular serotonin concentration (Fig. 2A). We also confirmed that paroxetine did not directly affect the L-Glu transport activity of the astrocyte culture (Fig. 2B). In our previous report, the down-regulation of GLAST in the inflammation model was caused by the elevation of extracellular L-Glu released from microglia (8). We therefore compared the effects of the antidepressants on LPS-induced L-Glu release from microglia. When microglia culture was treated with 10 ng/ml LPS for 24 h in the presence or absence of the antidepressants, only paroxetine suppressed L-Glu release in a concentration-dependent manner (Fig. 3A). The other antidepressants had no effects (Fig. 3B–E). We confirmed that paroxetine did not affect the microglial viability until 10 μM by LDH assay (data not shown). These results strongly suggest that the protective effect of paroxetine on the LPS-induced down-regulation of astrocytic L-Glu transporters was caused by the suppression of L-Glu release from microglia.

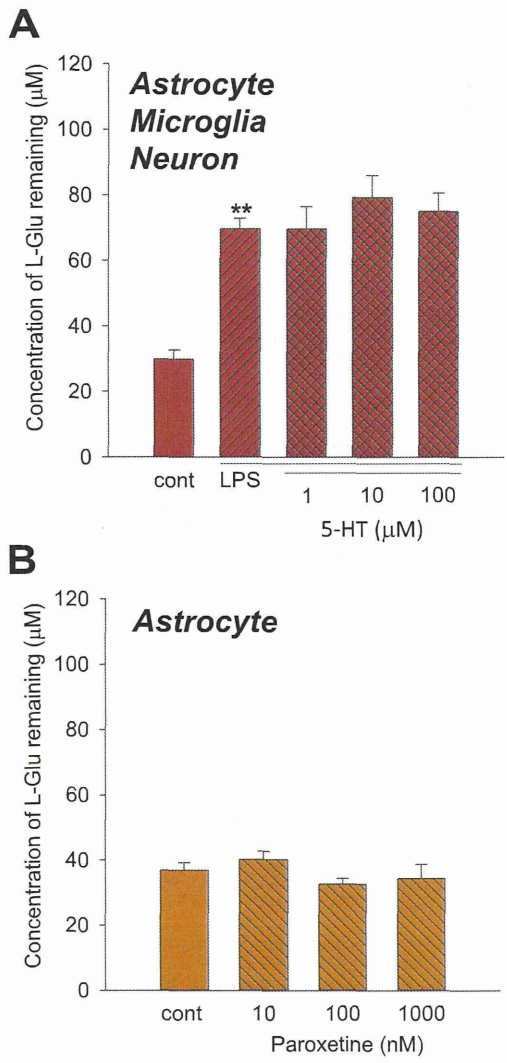

Fig. 2. Relation of the effects of paroxetine on LPS-induced decrease in L-Glu transport activity with its SSRI function and the direct effect on astrocytes. A. 72 h treatment with 5-HT (1–100 μM) did not affect LPS-induced decrease in the L-Glu transport activity. B. 72 h treatment with paroxetine (10–1000 nM) of astrocyte culture did not affect its L-Glu transport activity. **: $p < 0.01$ vs. control group, Tukey's test following ANOVA ($N = 6$).

The shape of microglia in the mixed culture was dramatically changed to amoeboid type by LPS and this morphological change was remarkably suppressed by paroxetine (unpublished observation). This suggests that paroxetine does not only suppress L-Glu release from microglia alone but also microglial activation. To demonstrate this possibility, the effect of paroxetine on the microglial activation is needed to be confirmed using multiple parameters. Because SSRIs have diverse chemical structures despite a common mode of action of 5-HT function (11), it is possible that paroxetine revealed the effects through interaction with paroxetine-specific target molecules. Because paroxetine exhibited the powerful inhibition of calcium influx via $P2X_4$ receptors (12), $P2X_4$ receptor is one of the most probable candidate molecules. The expression level of $P2X_4$ receptor in microglia is up-regulated in inflammatory pain model in spinal cord and is thought to be important for microglial inflammatory responses (13). MAPK signaling molecules (14) and GABA(B) receptor (15) are possibly involved in the paroxetine-specific effects as well. The effective concentration of paroxetine to reduce L-Glu release was 1 μM. According to the attached documents of paroxetine (http://www.info.pmda.go.jp/), intracerebral concentration of paroxetine reaches 77 nM by 25 mg/day-repeated administration. It is therefore unlikely that paroxetine affects astrocyte L-Glu transporters and microglia by the general dosage of SSRI. For clinical application of our present findings, further investigation concerning application period and dosage is needed.

Please cite this article in press as: Fujimori K, et al., Paroxetine prevented the down-regulation of astrocytic L-Glu transporters in neuroinflammation, Journal of Pharmacological Sciences (2014), http://dx.doi.org/10.1016/j.jphs.2014.09.002

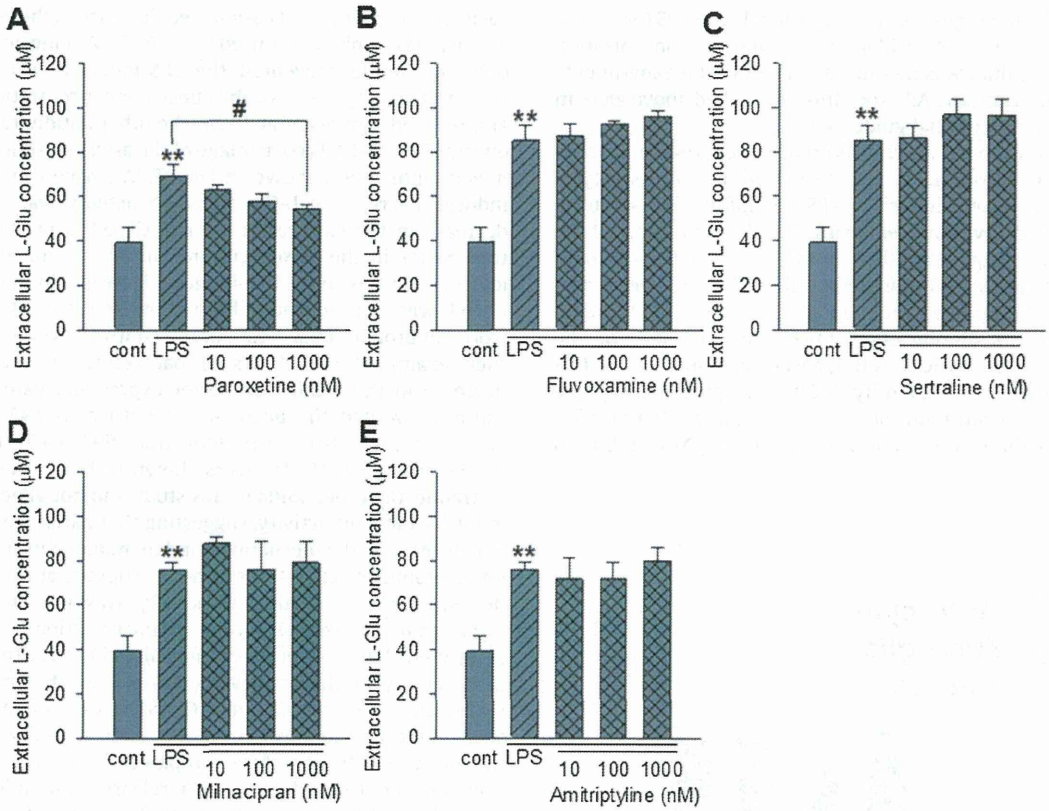

Fig. 3. Effects of antidepressants on the L-Glu release from microglia under the inflammatory condition. In each set of experiment, antidepressants were applied to the mixed culture from 1 h before to the end of the LPS-treatment (10 ng/ml, 24 h). The extracellular concentration of L-Glu was quantified. Paroxetine prevented the LPS-induced L-Glu release from microglia in a concentration-dependent manner (A). Fluvoxamine (B), sertraline (C), milnacipran (D), and amitriptyline (E) had no effects on LPS-induced L-Glu release from microglia. **: $p < 0.01$ vs. control group, #: $p < 0.05$ vs. LPS-treated group, Tukey's test following ANOVA ($N = 6$).

In conclusion, we found that paroxetine inhibit the L-Glu release from activated microglia and prevent down-regulation of astrocytic L-Glu transporters in the early stage of neuroinflammation. This is the novel pharmacological effect of paroxetine, which may bring advantages on the therapy of the disease associated with neuroinflammation.

Conflicts of interest

I declare that I have no significant competing financial, professional or personal interests that might have influenced the results and interpretation of the manuscript.

Author's contributions

K.F. performed experiments and manuscript writing.
J.T. performed experiments.
Y.S-M. provided advice on manuscript writing
Y.S. provided advice on manuscript writing
T.S. provided advice on the experimental direction and manuscript writing.
K.S. designed the experimental plan and performed experiments, manuscript writing.

Acknowledgments

This work was partly supported by a Grant-in-Aid for Young Scientists from Ministry of Education, Culture, Sports, Science, and Technology, Japan (KAKENHI 21700422), the Program for Promotion of Fundamental Studies in Health Sciences of National Institute of Biomedical Innovaton (10-21), Japan, a Health and Labor Science Research Grant for Research on Risks of Chemicals, a Labor Science Research Grant for Research on New Drug Development from the MHLW, Japan, awarded to K.S., Grant-in-Aid for research from MEXT, Japan (KAKENHI C23590113) awarded to T.S., and a Health and Labor Science Research Grant for Research on Publicly Essential Drugs and Medical Devices, Japan, awarded to Y.S.

References

(1) Bowerman M, Vincent T, Scamps F, Perrin FE, Camu W, Raoul C. Neuroimmunity dynamics and the development of therapeutic strategies for amyotrophic lateral sclerosis. Front Cell Neurosci. 2013;7:214.
(2) Liimatainen S, Lehtimaki K, Palmio J, Alapirtti T, Peltola J. Immunological perspectives of temporal lobe seizures. J Neuroimmunol. 2013;263:1–7.
(3) Schwartz M, Baruch K. The resolution of neuroinflammation in neurodegeneration: leukocyte recruitment via the choroid plexus. EMBO J. 2014;33:7–22.
(4) Lucas SM, Rothwell NJ, Gibson RM. The role of inflammation in CNS injury and disease. Br J Pharmacol. 2006;147(Suppl. 1):S232–S240.
(5) Masliah E, Alford M, DeTeresa R, Mallory M, Hansen L. Deficient glutamate transport is associated with neurodegeneration in Alzheimer's disease. Ann Neurol. 1996;40:759–766.
(6) Ferrarese C, Zoia C, Pecora N, Piolti R, Frigo M, Bianchi G, et al. Reduced platelet glutamate uptake in Parkinson's disease. J Neural Transm. 1999;106:685–692.
(7) Rothstein JD, Martin LJ, Kuncl RW. Decreased glutamate transport by the brain and spinal cord in amyotrophic lateral sclerosis. N Engl J Med. 1992;326:1464–1468.
(8) Takaki J, Fujimori K, Miura M, Suzuki T, Sekino Y, Sato K. L-glutamate released from activated microglia downregulates astrocytic L-glutamate transporter

Please cite this article in press as: Fujimori K, et al., Paroxetine prevented the down-regulation of astrocytic L-Glu transporters in neuroinflammation, Journal of Pharmacological Sciences (2014), http://dx.doi.org/10.1016/j.jphs.2014.09.002

expression in neuroinflammation: the 'collusion' hypothesis for increased extracellular L-glutamate concentration in neuroinflammation. J Neuroinflammation. 2012;9:275.
(9) Hashioka S, Klegeris A, Monji A, Kato T, Sawada M, McGeer PL, et al. Antidepressants inhibit interferon-gamma-induced microglial production of IL-6 and nitric oxide. Exp Neurol. 2007;206:33–42.
(10) Hwang J, Zheng LT, Ock J, Lee MG, Kim SH, Lee HW, et al. Inhibition of glial inflammatory activation and neurotoxicity by tricyclic antidepressants. Neuropharmacology. 2008;55:826–834.
(11) RJ B. Drugs and the treatment of psychiatrc disorders. Goodman and Gilman's the pharmacological basis of therapeutics. In: Hardman JG, Limbird LE, Gilman AG, editors. 10th ed 2001. p. 447–483.
(12) Nagata K, Imai T, Yamashita T, Tsuda M, Tozaki-Saitoh H, Inoue K. Antidepressants inhibit P2X4 receptor function: a possible involvement in neuropathic pain relief. Mol Pain. 2009;5:20.
(13) Guo LH, Trautmann K, Schluesener HJ. Expression of P2X4 receptor by lesional activated microglia during formalin-induced inflammatory pain. J Neuroimmunol. 2005;163:120–127.
(14) Liu RP, Zou M, Wang JY, Zhu JJ, Lai JM, Zhou LL, et al. Paroxetine ameliorates lipopolysaccharide-induced microglia activation via differential regulation of MAPK signaling. J Neuroinflammation. 2014;11:47.
(15) Khundakar AA, Zetterstrom TS. Effects of GABAB ligands alone and in combination with paroxetine on hippocampal BDNF gene expression. Eur J Pharmacol. 2011;671:33–38.

Please cite this article in press as: Fujimori K, et al., Paroxetine prevented the down-regulation of astrocytic L-Glu transporters in neuroinflammation, Journal of Pharmacological Sciences (2014), http://dx.doi.org/10.1016/j.jphs.2014.09.002

Fundamental Toxicological Sciences (Fund. Toxicol. Sci.)
Vol.1, No.3, 87-94, 2014

Original Article

Residual metals in carbon nanotubes suppress the proliferation of neural stem cells

Yukari Shigemoto-Mogami[1], Koki Fujimori[1,2], Yoshiaki Ikarashi[3], Akihiko Hirose[4], Yuko Sekino[1] and Kaoru Sato[1]

[1]*Laboratory of Neuropharmacology, Division of Pharmacology, National Institute of Health Sciences, 1-18-1 Kamiyoga, Setagaya-ku, Tokyo 158-8501, Japan*
[2]*Division of Basic Biological Science, Faculty of Pharmacy, Keio University, 1-5-30 Shiba-koen, Minato-ku, Tokyo 105-8512, Japan*
[3]*Division of Environmental Chemistry, National Institute of Health Sciences, 1-18-1 Kamiyoga, Setagaya-ku, Tokyo 158-8501, Japan*
[4]*Division of Risk Assessment, National Institute of Health Sciences, 1-18-1 Kamiyoga, Setagaya-ku, Tokyo 158-8501, Japan*

(Received October 17, 2014; Accepted October 20, 2014)

ABSTRACT — Carbon nanotubes (CNTs) are used in many fields; however, little is known about the effects of CNTs on the central nervous system (CNS). In this study, we found that extracts of sonicated CNTs suppressed the proliferation of neural stem cells (NSCs). Single-walled CNTs (SWCNTs) and multiple-walled CNTs (MWCNTs) were suspended in PBS (1 mg/mL) and sonicated for 5 hr using a water bath sonicator. Supernatants from both types of CNTs suppressed NSC proliferation. The effects weakened in a dilution-ratio-dependent manner and strengthened in a sonication time-dependent manner. Metal concentrations extracted from SCNTs and MCNTs after 5-hr of sonication were determined using inductively coupled plasma mass spectrometry. Mn, Rb, Cs, Tl, and Fe were detected in the SWCNT supernatant, and Mn, Cs, W, and Tl were detected in the MWCNT supernatant. The concentration of Mn, Rb, and Fe eluted from the SWCNTs and Rb eluted from MWCNTs following sonication were sufficient to suppress NSC proliferation alone. N-acetyl cysteine (NAC) and ascorbic acid (AA) reversed the effects of Mn and Fe and restored NSC proliferation. The effects of Rb and Tl were not affected by the antioxidants. Both antioxidants largely restored the suppression of NSC proliferation induced by the SWCNT and MWCNT supernatants. These results suggest that metals extracted from CNTs via a strong vibration energy can suppress NSC proliferation through ROS production by the extracted metals.

Key words: Carbon nanotube, Neural stem cell, Metals, Proliferation

INTRODUCTION

CNTs are fiber-shaped nanomaterials that consist of graphite hexagonal-mesh planes (graphene sheet) in a single-layer (single-walled carbon nanotubes (SWCNTs)) or in multiple layers with nest accumulation (multi-walled carbon nanotubes (MWCNTs)). The structure of SWCNTs is a honeycomb carbon lattice rolled into a cylinder, and the basic morphology consists of a sheet of tangled SWCNT (with a diameter of approximately 2 nm) bundles with diameters tens of nanometers in length. The structure of MWCNTs consists of honeycomb carbon lattices rolled into a multi-layer tubular shape, and the basic morphology is composed of particles of tangled MWCNTs with a diameter of approximately 30 nm. CNTs are used in many fields, including energy, healthcare, environment, materials, and electronics. However, adverse effects of CNTs on human health are poorly understood. Exposure to asbestos is known to cause asbestosis, bronchogenic carcinoma, mesothelioma, pleural fibrosis and pleural plaques, indicating that both the lungs and the pleura are targets of asbestos (Donaldson *et al.*, 2013). CNTs also exist as fibers or compact particles; thus, most studies concerning the adverse effects of CNTs have focused on lung toxicity (Jaurand *et al.*, 2009; Pacurari *et al.*, 2010) based on the fiber pathogenicity paradigm developed in the 1970-80s.

Correspondence: Kaoru Sato (E-mail: kasato@nihs.go.jp)

However, recent reports showed that nano-particles can cross the blood–brain barrier (BBB) and enter the brain (Sharma and Sharma, 2007). Furthermore, it has been suggested that the olfactory nerve pathway is a portal of entry into the CNS (Henriksson and Tjalve, 2000; Persson *et al.*, 2003; Mistry *et al.*, 2009; Balasubramanian *et al.*, 2013). Recent reports showed that MWCNTs are toxic to neural cells (Belyanskaya *et al.*, 2009; Xu *et al.*, 2009; Gavello *et al.*, 2012). Here, we investigated the effects of CNTs on the self-renewal of neural stem cells (NSCs). The mammalian CNS comprises various cell types, including neurons, astrocytes, and oligodendrocytes, and these cells differentiate from NSCs at specific brain developmental stages. Sufficient proliferation of NSCs before differentiation is essential to supply the neurons and glia required for brain function (Caviness *et al.*, 1995; Kriegstein and Alvarez-Buylla, 2009). In addition, NSCs are maintained in the subventricular zone and the hippocampal subgranular zone in the adult brain. Adult neurogenesis from these NSCs plays a key role in higher-order brain functions, such as cognition, learning and memory (Couillard-Despres *et al.*, 2011; Eisch and Petrik, 2012; Rolando and Taylor, 2014). Thus, the effects of CNTs on the proliferation of NSCs need to be determined for both of brain development and brain function. Here, we report that sonicated extracts of CNTs suppressed the proliferation of NSCs. We also determined that these effects were mediated through ROS produced by residual metals in the CNTs.

MATERIALS AND METHODS

Materials

CNTs (SWCNT: purity > 95%; Lot No.: SW1859; MWCNT: purity: > 98%; Lot No.: 04-12/10#1-(4)) were supplied by Nikkiso Co., Ltd. (Shizuoka, Japan). Both test materials were not coated or modified. The detailed physiochemical properties of Nikkiso CNTs have been previously reported (Ema *et al.*, 2011; Matsumoto *et al.*, 2012). Epidermal growth factor (EGF), $MnCl_2$, RbCl, $TlCl_3$, $FeCl_2$, $FeCl_3$, and NAC were purchased from Sigma (St. Louis, Mo, USA). Fibroblast growth factor 2 (FGF2) was purchased from PeproTech (Rocky Hill, NJ, USA). AA was purchased from WAKO (Osaka, Japan). The BrdU cell proliferation assay kit was purchased from Merck (Darmstadt, Germany). B27 supplement, TrypLE Select, FBS, and DMEM were purchased from Life Technologies (Grand Island, NY, USA).

Preparation of supernatants of sonicated CNT solutions

SWCNTs and MWCNTs were suspended in PBS (1 mg/mL) and sonicated for 10 min or 5 hr using a water bath-sonicator (Hitachi-Kokusai Electric Inc., Tokyo, Japan) at a frequency of 36 kHz and a watt density of 65 W/264 cm^2. The supernatants of sonicated CNT suspensions were diluted with culture medium 10- to 1,000-fold.

Rat neural stem cell (NSC) culture

Rat NSCs were cultured as previously described (Reynolds *et al.*, 1992; Hamanoue *et al.*, 2009) with slight modifications. Briefly, the telencephalons were dissected from embryonic day 16 (E16) rats of either sex in ice-cold DMEM/F12. The tissue was then minced and dispersed into single cells by pipetting. Cells were then cultured in DMEM/F12 containing B27 supplement (1/200), 20 ng/mL fibroblast growth factor 2 (FGF2) and 20 ng/mL epidermal growth factor (EGF) for 7 days. The primary neurospheres were incubated with TrypLE Select for 15 min and dissociated by pipetting. Single cells were seeded in 96-well plates for the proliferation assay.

Measurement of metal concentrations

CNTs were suspended in PBS (1 mg/mL) and sonicated for 5 hr using a water bath sonicator. The metal concentrations in the CNT supernatants were quantified using an inductively coupled plasma mass spectrometer (ICP-MS) (Agilent 7500ce ICP-MS, Agilent Technologies, Santa Clara, CA, USA) fitted with a collision/reaction cell in helium mode. We first detected metals at concentrations exceeding the detection limits using a semi-quantitative analysis. Next, we determined the concentration of the detected metals (i.e., Mn, Fe, Rb, Cs, W, and Tl) using a full quantitative analysis with calibration curves.

Treatment of NSCs with the supernatants of sonicated CNT suspensions, metals, and antioxidants

NSCs were treated with the supernatants of sonicated CNT suspensions, $MnCl_2$ (1-100 ppb), RbCl (1-100 ppb), $TlCl_3$ (0.1-10 ppb), $FeCl_2$ (100-10,000 ppb) or $FeCl_3$ (100-10,000 ppb) with or without 10 μM N-acetyl cysteine (NAC) or 10 μM ascorbic acid (AA) for 24 hr.

NSC proliferation assay

We quantified NSC proliferation according the instructions from the BrdU cell proliferation assay kit (Calbiochem, Hayward, CA, USA). The primary neurospheres were dissociated into single cells and seeded in 96-well plates at a density of 2 x 10^4 cells/

well. BrdU was added to the medium during the treatment of NSCs. After incubation, the cells were fixed, and BrdU-immuno-labeling was performed. The fluorescence intensities were used as a marker of proliferation. The fluorescence was measured at an excitation wavelength of 320 nm and emission wavelength of 460 nm with a fluorescence microplate reader (Spectra Max Microplate reader, Molecular Devices, Sunnyvale, CA, USA).

Data analysis and statistics

All data are shown as the mean ± S.E.M. The statistical analysis was performed using Student's *t*-test or an ANOVA followed by a Tukey's test. Differences were considered to be significant at $p < 0.05$.

RESULTS

SWCNTs and MWCNTs were suspended in PBS (1 mg/mL) and sonicated for 5 hr using a water bath sonicator. The supernatants of the sonicated CNT suspensions were collected and diluted with culture medium 10- to 1,000-fold. We found that a 24-hr treatment with supernatants of SWCNT and MWCNT suppressed NSC proliferation in a dilution ratio-dependent manner (Fig. 1). The suppression of proliferation was stronger with the SWCNT supernatant when compared with the MWCNT supernatant. The effects of sonication time were also assessed. The suppressive effects of both supernatants disappeared when the sonication time was changed from 5 hr to 10 min (Fig. 2). These results suggest that the suppression of NSC proliferation is due to factors released from CNTs in a sonication time-dependent manner.

CNTs are manufactured using metallic catalysts (Ding *et al.*, 2008; Yazyev and Pasquarello, 2008; Banhart, 2009; Tyagi *et al.*, 2011). Thus, we speculated that residual metals extracted from CNTs during the 5-hr sonication may be responsible for the suppression of NSC proliferation. We therefore quantified the metal contents in the CNT supernatants. The metals in the SWCNT and MWCNT supernatants were first analyzed using ICP-MS in a semi-quantitative mode. Next, the concentrations of metals were determined using calibration curves (Table 1). We found that a 5-hr sonication induced the extraction of multiple metals from the CNTs. Mn, Rb, Cs, Tl, and Fe were detected in the SWCNT supernatant, whereas Mn, Cs, W, and Tl were detected in the MWCNT supernatant. Among these metals, the concentration of Fe in SWCNT supernatant was remarkably high (from N.D. to 7,110 ppb). The concentrations of these metals in PBS were largely negligible and did not change after a 5-hr sonication.

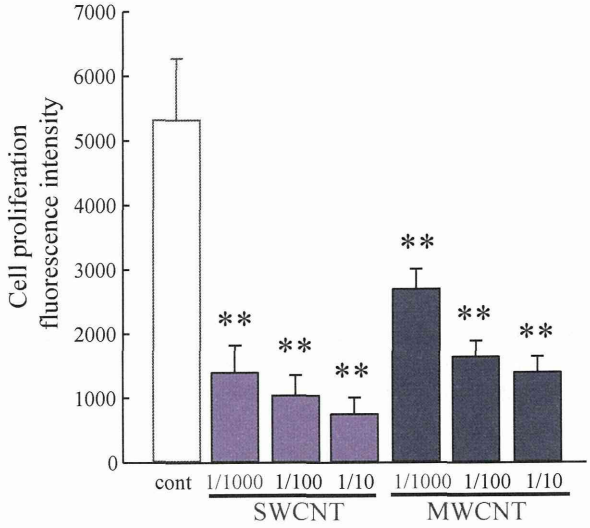

Fig. 1. Effects of the supernatants of sonicated CNT suspensions on the proliferation of rat NSCs. The supernatants of SWCNTs and MWCNTs suppressed NSC proliferation in a dilution ratio-dependent manner. *: $p < 0.05$, **: $p < 0.01$ vs. control group ($N = 6$), ANOVA followed by a Tukey's test.

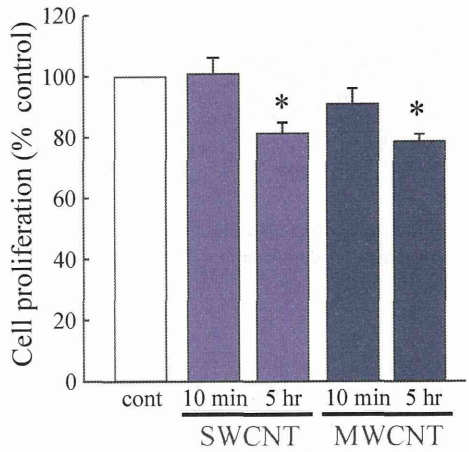

Fig. 2. Sonication time-dependence of CNT supernatant effects. The effects of SWCNT and MWCNT supernatants disappeared with a sonication time of 10 min. However, a 5-hr sonication time produced a significant suppression of NSC proliferation. *: $p < 0.05$ vs. control group ($N = 6$), ANOVA followed by a Tukey's test.

Next, we examined the direct effects of the metals at concentration ranges detected in the supernatants. Fig. 3 shows the metals that had a suppressive effect on NSC

Table 1. Metals eluted from CNTs by sonication for 5 hr.

	Concentrations of metals (ppb) 1 ppb = 10^{-8}%					
	PBS	PBS	SWCNT	SWCNT	MWCNT	MWCNT
sonication	-	+	-	+	-	+
Mn	nd	nd	0.33	16.04	nd	0.26
Rb	3.97	3.84	6.88	13.33	4.06	4.61
Cs	nd	nd	0.1	0.32	nd	0.59
W	nd	0.05	nd	0.08	nd	0.4
Tl	md	nd	0.05	0.17	nd	0.37
Fe	nd	nd	nd	7110	nd	nd

The metal concentrations in the supernatant of SWCNT and MWCNT were quantified using ICP-MS in a semi-quantitative mode followed by a full quantitative mode. Mn, Rb, Cs, W, Tl, and Fe were detected in the SWCNT supernatant. Mn, Rb, Cs, W, Tl, and Fe were detected in the MWCNT supernatant. The concentration of Fe in the SWCNT supernatant was remarkably high (7,110 ppb).

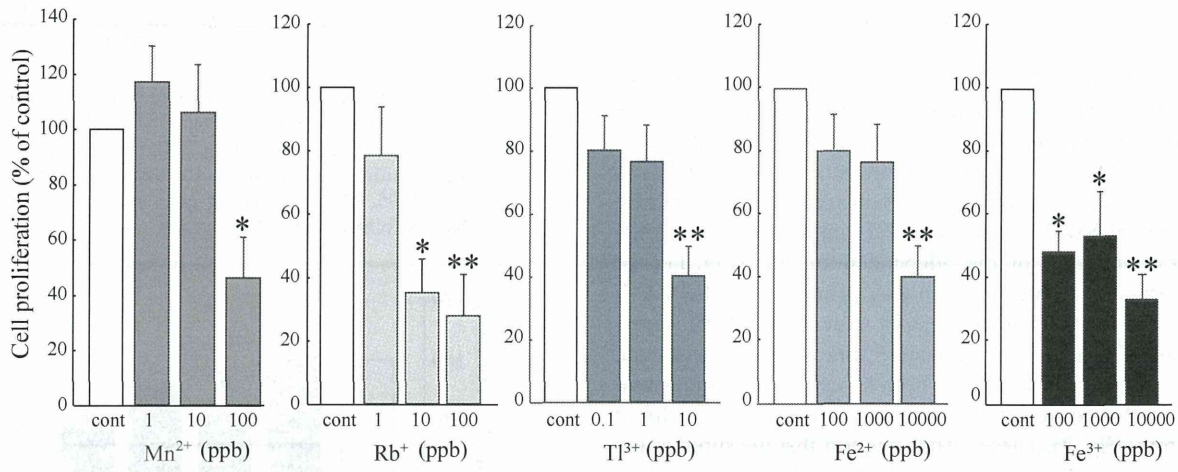

Fig. 3. The direct effect of metals in CNT supernatants. Mn^{2+}, Rb^{+}, Tl^{3+}, Fe^{2+}, and Fe^{3+} suppressed NSC proliferation in a concentration-dependent manner. *: $p < 0.05$, **: $p < 0.01$ vs. control group (N = 12). ANOVA followed by a Tukey's test.

proliferation (Fig. 3). Mn^{2+}, Rb^{+}, Tl^{3+}, Fe^{2+}, and Fe^{3+} suppressed the proliferation of NSCs in a concentration-dependent manner. These results indicate that Mn, Rb, and Fe were present in the SWCNT supernatant at a concentration high enough to suppress NSC proliferation. This effect was induced by the Rb in the MWCNT supernatant. Some metals are known to produce reactive oxygen species (Ding *et al.*, 2008) that can result in oxidative stress on lipids, DNA and proteins (Henriksson and Tjalve, 2000; Choi *et al.*, 2007; Alekseenko *et al.*, 2008; Kim *et al.*, 2011; Latronico *et al.*, 2013; Roth and Eichhorn, 2013; Sripetchwandee *et al.*, 2013). Thus, we examined the involvement of ROS in the suppression of NSC proliferation. N-acetyl cysteine (NAC) (10 μM) and ascorbic acid (AA) (10 μM) are typical antioxidants that can significantly restore the suppression of the NSC proliferation caused by Mn^{2+}, Fe^{2+}, and Fe^{3+} (Fig. 4A). The effect of Rb and Tl were not affected by NAC or AA (data not shown). These results suggest that ROS is involved in the suppressive effects produced by Mn and Fe. We also examined whether ROS played a role in the suppression of NSC proliferation by the CNT supernatants (Fig. 4B). Both NAC and AA markedly restored the decrease in NSC proliferation caused by the SWCNT and MWCNT supernatants. We confirmed that both of these antioxidants alone did not affect NSC proliferation (data not shown). Taken together, these results suggest that the suppressive effects of the sonicated extract of CNTs were mainly caused by

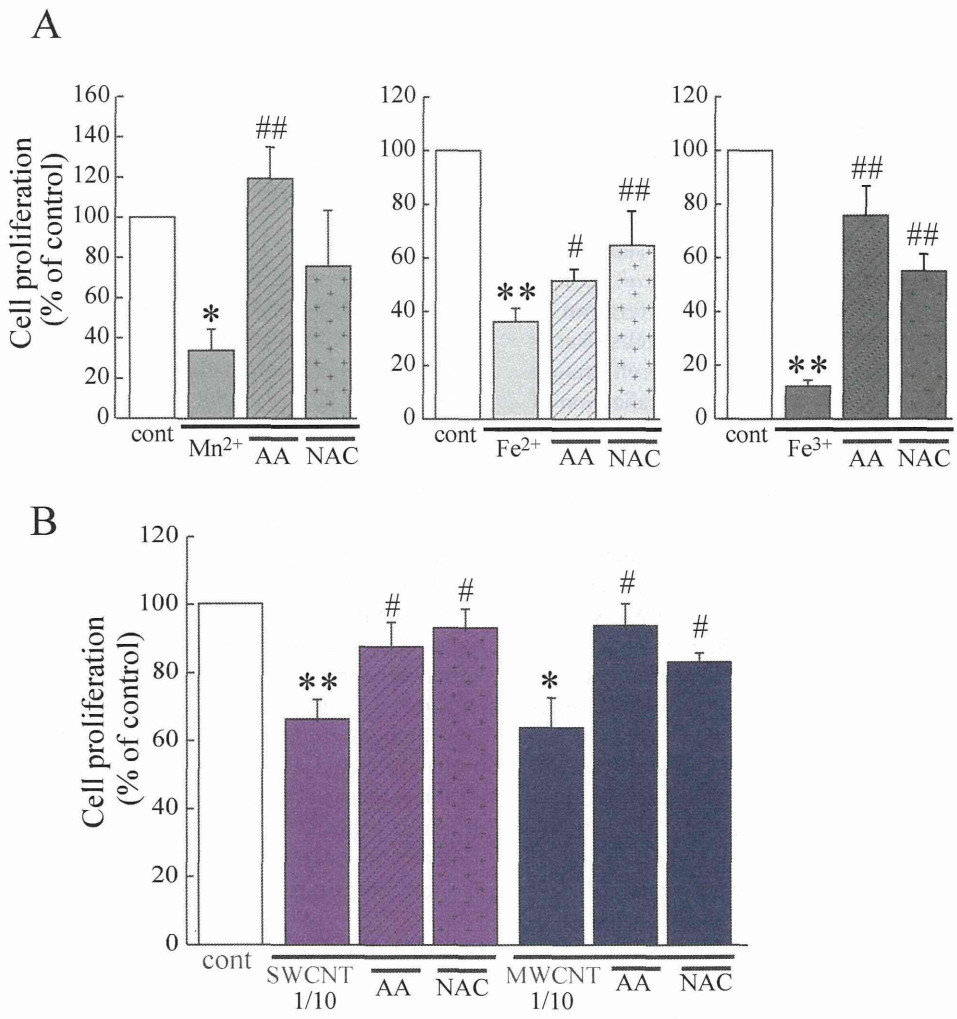

Fig. 4. Antioxidants attenuated the reduction in NSC proliferation caused by metals and CNT supernatants. The suppression of the NSC proliferation caused by Mn^{2+}, Fe^{2+}, Fe^{3+} (A) and the supernatants of CNTs (B) was significantly restored by NAC (10 μM) and AA (10 μM). *: $p < 0.05$,**: $p < 0.01$ vs. control group, #: $p < 0.05$, ##: $p < 0.01$ vs. metal or CNT-supernatant-treated groups (N = 7), ANOVA followed by a Tukey's test.

ROS produced by residual metals.

DISCUSSION

We found that the supernatants of sonicated CNT suspensions suppress NSC proliferation. We also determined that these effects were largely mediated by ROS production from residual metals. To demonstrate the involvement of ROS, we used the two antioxidants NAC and AA. NAC exerts its protective by increasing glutathione levels (Yim *et al.*, 1994; Arfsten *et al.*, 2007; Li *et al.*, 2009), directly scavenging ROS, and activating ERK1/2 (Zhang *et al.*, 2011). AA is a powerful water-soluble antioxidant that acts by scavenging ROS and reactive nitrogen species (Carr and Frei, 1999; Kojo, 2004). The concentrations of NAC and AA used in this study were at a level shown to suppress the effects of ROS in previous studies (Carr and Frei, 1999; De la Fuente and Victor, 2001; Nakajima *et al.*, 2009).

Proliferative NSCs have a high endogenous ROS lev-

el (Le Belle *et al.*, 2011), and redox balance is important to regulate NSC/neural progenitor cell (NPC)-self-renewal and differentiation (Smith *et al.*, 2000; Li *et al.*, 2007; Hou *et al.*, 2012; Topchiy *et al.*, 2013). For example, mitochondrial superoxide negatively regulates NPC-self-renewal in the developmental cerebral cortex (Hou *et al.*, 2012). High levels of ROS inhibit O-2A progenitor proliferation (Smith *et al.*, 2000; Li *et al.*, 2007). In other cases, NADPH oxidase (Nox) 4-generated superoxide drives mouse NSC proliferation (Topchiy *et al.*, 2013). Ketamine-induced ROS enhanced the proliferation of NSCs derived from human embryonic stem cells (Bai *et al.*, 2013). The effect of ROS on NSC/NPC proliferation may change depending on the subcellular localization of the ROS generation and the timing of the ROS generation.

The suppression of NSC proliferation by the supernatants of both CNTs were virtually restored by the antioxidants, suggesting that the effects of CNT-supernatants were mediated through ROS stress. After a 5-hr sonication, multiple metals were detected in the SWCNT and MWCNT supernatants using ICP-MS. Mn, Rb, Cs, Tl, and Fe were detected in the SWCNT supernatant, and Mn, Cs, W, and Tl were detected in the MWCNT supernatant. Out of these SWCNT metals, the effects of Mn and Fe were reversed by antioxidants, suggesting that Mn and Fe play the main role in the suppression of NSC proliferation by CNT supernatants. In the MWCNT supernatant, the concentrations of Mn and Fe were insufficient to suppress NSC proliferation. Thus, a combination of ROS produced by multiple metals might produce synergistic suppressive effects.

Fe is essential for biological processes, but it is also known to be toxic in excess. Fe^{2+} overload into the cells and shuttling of Fe^{2+} to Fe^{3+} leads to cellular malfunctions due to ROS production (Halliwell and Gutteridge, 1992; Touati, 2000). Although Fe^{3+} has been largely considered as non-cytotoxic (Braun, 1997; Bruins *et al.*, 2000), it has its own mechanisms that can alter cell viability (Chamnongpol *et al.*, 2002). Fe^{3+} shows ROS production even while bound to proteins (Alekseenko *et al.*, 2008). GSH revealed pro-oxidant effects in the presence of an exogenous Fe^{3+} (Zager and Burkhart, 1998). Furthermore, Fe^{2+} and Fe^{3+} were shown to enter brain mitochondria and cause mitochondrial depolarization and ROS production (Sripetchwandee *et al.*, 2013). Mn is also essential for biological processes, but it has been known to be a neurotoxicant in excess. Mn induces oxidative stress (Choi *et al.*, 2007; Park and Park, 2010) and the release of cytokines (Park and Park, 2010). Mn further potentiates inflammation by the release of MMP9 through ROS production and modulation of ERK (Latronico *et al.*, 2013). Rb was also detected in the supernatants of SWCNT and MWCNT. Here, we found that Rb alone suppressed NSC proliferation in a ROS-independent manner. Rb has long been considered as nontoxic. Rb is generally used as a medical contrast medium because of its long half-life. Thus, the mechanism behind the Rb effects should be clarified quickly.

Most commercial CNTs contain ultrafine metal particles composed of Fe, Ni, Y, Co, Pb, and Cu that are used as catalysts (Ding *et al.*, 2008; Yazyev and Pasquarello, 2008; Banhart, 2009; Tyagi *et al.*, 2011). Recent studies showed that metal impurities play a major role in CNT cytotoxicity (Liu *et al.*, 2008; Kim *et al.*, 2010). The residual metals can remain in the contact solvent or embed inside the CNTs (Pumera, 2007; Fubini *et al.*, 2011; Aldieri *et al.*, 2013). In our study, the content of Fe in SWCNT was remarkable. A SWCNT is a graphene sheet protected metal core/shell of nanoparticles (Pumera, 2007). This structure may have caused the higher levels of metal impurities when compared with MWCNTs. Our data suggest that the residual metallic catalysts are released by vibration energy with a sonication frequency of 36 kHz, watt density of 65 W/264 cm^2 and sonication time of 5 hr. Pumera *et al.* indicated that washing with concentrated nitric acid removed up to 88% (w/w) of metal catalyst nanoparticles (Pumera, 2007). For public health and the safer applications of CNTs in nano-medicine, it is preferable to decrease the amount of the metal impurities by improving the washing process.

Conflict of interest---- The authors declare that there is no conflict of interest.

REFERENCES

Aldieri, E., Fenoglio, I., Cesano, F., Gazzano, E., Gulino, G., Scarano, D., Attanasio, A., Mazzucco, G., Ghigo, D. and Fubini, B. (2013): The role of iron impurities in the toxic effects exerted by short multiwalled carbon nanotubes (MWCNT) in murine alveolar macrophages. J. Toxicol. Environ. Health Part A, **76**, 1056-1071.

Alekseenko, A.V., Waseem, T.V. and Fedorovich, S.V. (2008): Ferritin, a protein containing iron nanoparticles, induces reactive oxygen species formation and inhibits glutamate uptake in rat brain synaptosomes. Brain Res., **1241**, 193-200.

Arfsten, D.P., Johnson, E.W., Wilfong, E.R., Jung, A.E. and Bobb, A.J. (2007): Distribution of radio-labeled N-Acetyl-L-Cysteine in Sprague-Dawley rats and its effect on glutathione metabolism following single and repeat dosing by oral gavage. Cutan. Ocul. Toxicol., **26**, 113-134.

Bai, X., Yan, Y., Canfield, S., Muravyeva, M.Y., Kikuchi, C., Zaja, I., Corbett, J.A. and Bosnjak, Z.J. (2013): Ketamine enhances human neural stem cell proliferation and induces neuronal apop-

tosis via reactive oxygen species-mediated mitochondrial pathway. Anesth. Analg., **116**, 869-880.

Balasubramanian, S.K., Poh, K.W., Ong, C.N., Kreyling, W.G., Ong, W.Y. and Yu, L.E. (2013): The effect of primary particle size on biodistribution of inhaled gold nano-agglomerates. Biomaterials, **34**, 5439-5452.

Banhart, F. (2009): Interactions between metals and carbon nanotubes: at the interface between old and new materials. Nanoscale, **1**, 201-213.

Belyanskaya, L., Weigel, S., Hirsch, C., Tobler, U., Krug, H.F. and Wick, P. (2009): Effects of carbon nanotubes on primary neurons and glial cells. Neurotoxicology, **30**, 702-711.

Braun, V. (1997): Avoidance of iron toxicity through regulation of bacterial iron transport. Biol. Chem., **378**, 779-786.

Bruins, M.R., Kapil, S. and Oehme, F.W. (2000): Microbial resistance to metals in the environment. Ecotoxicol. Environ. Saf., **45**, 198-207.

Carr, A. and Frei, B. (1999): Does vitamin C act as a pro-oxidant under physiological conditions? FASEB J., **13**, 1007-1024.

Caviness, V.S.Jr., Takahashi, T. and Nowakowski, R.S. (1995): Numbers, time and neocortical neuronogenesis: a general developmental and evolutionary model. Trends Neurosci., **18**, 379-383.

Chamnongpol, S., Dodson, W., Cromie, M.J., Harris, Z.L. and Groisman, E.A. (2002): Fe(III)-mediated cellular toxicity. Mol. Microbiol., **45**, 711-719.

Choi, C.J., Anantharam, V., Saetveit, N.J., Houk, R.S., Kanthasamy, A. and Kanthasamy, A.G. (2007): Normal cellular prion protein protects against manganese-induced oxidative stress and apoptotic cell death. Toxicol. Sci., **98**, 495-509.

Couillard-Despres, S., Iglseder, B. and Aigner, L. (2011): Neurogenesis, cellular plasticity and cognition: the impact of stem cells in the adult and aging brain--a mini-review. Gerontology, **57**, 559-564.

De la Fuente, M. and Victor, V.M. (2001): Ascorbic acid and N-acetylcysteine improve *in vitro* the function of lymphocytes from mice with endotoxin-induced oxidative stress. Free Radic. Res., **35**, 73-84.

Ding, F., Larsson, P., Larsson, J.A., Ahuja, R., Duan, H., Rosen, A. and Bolton, K. (2008): The importance of strong carbon-metal adhesion for catalytic nucleation of single-walled carbon nanotubes. Nano Lett., **8**, 463-468.

Donaldson, K., Poland, C.A., Murphy, F.A., MacFarlane, M., Chernova, T. and Schinwald, A. (2013): Pulmonary toxicity of carbon nanotubes and asbestos - similarities and differences. Adv. Drug Deliv. Rev., **65**, 2078-2086.

Eisch, A.J. and Petrik, D. (2012): Depression and hippocampal neurogenesis: a road to remission? Science, **338**, 72-75.

Ema, M., Matsuda, A., Kobayashi, N., Naya, M. and Nakanishi, J. (2011): Evaluation of dermal and eye irritation and skin sensitization due to carbon nanotubes. Regul.Toxicol. Pharmacol., **61**, 276-281.

Fubini, B., Fenoglio, I., Tomatis, M. and Turci, F. (2011): Effect of chemical composition and state of the surface on the toxic response to high aspect ratio nanomaterials. Nanomedicine (Lond), **6**, 899-920.

Gavello, D., Vandael, D.H., Cesa, R., Premoselli, F., Marcantoni, A., Cesano, F., Scarano, D., Fubini, B., Carbone, E., Fenoglio, I. and Carabelli, V. (2012): Altered excitability of cultured chromaffin cells following exposure to multi-walled carbon nanotubes. Nanotoxicology, **6**, 47-60.

Halliwell, B. and Gutteridge, J.M. (1992): Biologically relevant metal ion-dependent hydroxyl radical generation. An update. FEBS Lett., **307**, 108-112.

Hamanoue, M., Matsuzaki, Y., Sato, K., Okano, H.J., Shibata, S., Sato, I., Suzuki, S., Ogawara, M., Takamatsu, K. and Okano, H. (2009): Cell surface N-glycans mediated isolation of mouse neural stem cells. J. Neurochem., **110**, 1575-1584.

Henriksson, J. and Tjalve, H. (2000): Manganese taken up into the CNS via the olfactory pathway in rats affects astrocytes. Toxicol. Sci., **55**, 392-398.

Hou, Y., Ouyang, X., Wan, R., Cheng, H., Mattson, M.P. and Cheng, A. (2012): Mitochondrial superoxide production negatively regulates neural progenitor proliferation and cerebral cortical development. Stem Cells, **30**, 2535-2547.

Jaurand, M.C., Renier, A. and Daubriac, J. (2009): Mesothelioma: Do asbestos and carbon nanotubes pose the same health risk? Part. Fibre Toxicol., **6**, 16.

Kim, J.E., Lim, H.T., Minai-Tehrani, A., Kwon, J.T., Shin, J.Y., Woo, C.G., Choi, M., Baek, J., Jeong, D.H., Ha, Y.C., Chae, C.H., Song, K.S., Ahn, K.H., Lee, J.H., Sung, H.J., Yu, I.J., Beck, G.R.Jr. and Cho, M.H. (2010): Toxicity and clearance of intratracheally administered multiwalled carbon nanotubes from murine lung. J. Toxicol. Environ. Health Part A, **73**, 1530-1543.

Kim, K.K., Singh, R.K., Strongin, R.M., Moore, R.G., Brard, L. and Lange, T.S. (2011): Organometallic iron(III)-salophene exerts cytotoxic properties in neuroblastoma cells via MAPK activation and ROS generation. PloS One, **6**, e19049.

Kojo, S. (2004): Vitamin C: basic metabolism and its function as an index of oxidative stress. Curr. Med. Chem., **11**, 1041-1064.

Kriegstein, A. and Alvarez-Buylla, A. (2009): The glial nature of embryonic and adult neural stem cells. Ann. Rev. Neurosci., **32**, 149-184.

Latronico, T., Brana, M.T., Merra, E., Fasano, A., Di Bari, G., Casalino, E. and Liuzzi, G.M. (2013): Impact of manganese neurotoxicity on MMP-9 production and superoxide dismutase activity in rat primary astrocytes. Effect of resveratrol and therapeutical implications for the treatment of CNS diseases. Toxicol. Sci., **135**, 218-228.

Le Belle, J.E., Orozco, N.M., Paucar, A.A., Saxe, J.P., Mottahedeh, J., Pyle, A.D., Wu, H. and Kornblum, H.I. (2011): Proliferative neural stem cells have high endogenous ROS levels that regulate self-renewal and neurogenesis in a PI3K/Akt-dependant manner. Cell Stem Cell, **8**, 59-71.

Li, W., Nie, S., Yu, Q. and Xie, M. (2009): (-)-Epigallocatechin-3-gallate induces apoptosis of human hepatoma cells by mitochondrial pathways related to reactive oxygen species. J. Agric. Food Chem., **57**, 6685-6691.

Li, Z., Dong, T., Proschel, C. and Noble, M. (2007): Chemically diverse toxicants converge on Fyn and c-Cbl to disrupt precursor cell function. PLoS Biol., **5**, e35.

Liu, X., Guo, L., Morris, D., Kane, A.B. and Hurt, R.H. (2008): Targeted Removal of Bioavailable Metal as a Detoxification Strategy for Carbon Nanotubes. Carbon, **46**, 489-500.

Matsumoto, M., Serizawa, H., Sunaga, M., Kato, H., Takahashi, M., Hirata-Koizumi, M., Ono, A., Kamata, E. and Hirose, A. (2012): No toxicological effects on acute and repeated oral gavage doses of single-wall or multi-wall carbon nanotube in rats. J. Toxicol. Sci., **37**, 463-474.

Mistry, A., Stolnik, S. and Illum, L. (2009): Nanoparticles for direct nose-to-brain delivery of drugs. Int. J. Pharm., **379**, 146-157.

Nakajima, Y., Tsuruma, K., Shimazawa, M., Mishima, S. and Hara, H. (2009): Comparison of bee products based on assays of antioxidant capacities. BMC Complement. Altern. Med., **9**, 4.

Pacurari, M., Castranova, V. and Vallyathan, V. (2010): Single- and multi-wall carbon nanotubes versus asbestos: are the carbon nanotubes a new health risk to humans? J. Toxicol. Environ. Health A., **73**, 378-395.

Park, E.J. and Park, K. (2010): Induction of oxidative stress and inflammatory cytokines by manganese chloride in cultured T98G cells, human brain glioblastoma cell line. Toxicol. In Vitro, **24**, 472-479.

Persson, E., Henriksson, J. and Tjalve, H. (2003): Uptake of cobalt from the nasal mucosa into the brain via olfactory pathways in rats. Toxicol. Lett., **145**, 19-27.

Pumera, M. (2007): Carbon nanotubes contain residual metal catalyst nanoparticles even after washing with nitric acid at elevated temperature because these metal nanoparticles are sheathed by several graphene sheets. Langmuir, **23**, 6453-6458.

Reynolds, B.A., Tetzlaff, W. and Weiss, S. (1992): A multipotent EGF-responsive striatal embryonic progenitor cell produces neurons and astrocytes. J. Neurosci., **12**, 4565-4574.

Rolando, C. and Taylor, V. (2014): Neural stem cell of the hippocampus: development, physiology regulation, and dysfunction in disease. Curr Top Dev Biol., **107**, 183-206.

Roth, J.A. and Eichhorn, M. (2013): Down-regulation of LRRK2 in control and DAT transfected HEK cells increases manganese-induced oxidative stress and cell toxicity. Neurotoxicology, **37**, 100-107.

Sharma, H.S. and Sharma, A. (2007): Nanoparticles aggravate heat stress induced cognitive deficits, blood-brain barrier disruption, edema formation and brain pathology. Prog. Brain Res., **162**, 245-273.

Smith, J., Ladi, E., Mayer-Proschel, M. and Noble, M. (2000): Redox state is a central modulator of the balance between self-renewal and differentiation in a dividing glial precursor cell. Proceedings of the National Academy of Sciences of the United States of America, **97**, 10032-10037.

Sripetchwandee, J., Sanit, J., Chattipakorn, N. and Chattipakorn, S.C. (2013): Mitochondrial calcium uniporter blocker effectively prevents brain mitochondrial dysfunction caused by iron overload. Life Sci., **92**, 298-304.

Topchiy, E., Panzhinskiy, E., Griffin, W.S., Barger, S.W., Das, M. and Zawada, W.M. (2013): Nox4-generated superoxide drives angiotensin II-induced neural stem cell proliferation. Dev. Neurosci., **35**, 293-305.

Touati, D. (2000): Iron and oxidative stress in bacteria. Arch. Biochem. Biophys., **373**, 1-6.

Tyagi, P.K., Janowska, I., Cretu, O., Pham-Huu, C. and Banhart, F. (2011): Catalytic action of gold and copper crystals in the growth of carbon nanotubes. J. Nanosci. Nanotechnol., **11**, 3609-3615.

Xu, L.J., Zhao, J.X., Zhang, T., Ren, G.G. and Yang, Z. (2009): *In vitro* study on influence of nano particles of CuO on CA1 pyramidal neurons of rat hippocampus potassium currents. Environ. Toxicol., **24**, 211-217.

Yazyev, O.V. and Pasquarello, A. (2008): Effect of metal elements in catalytic growth of carbon nanotubes. Phys. Rev. Lett., **100**, 156102.

Yim, M.B., Chae, H.Z., Rhee, S.G., Chock, P.B. and Stadtman, E.R. (1994): On the protective mechanism of the thiol-specific antioxidant enzyme against the oxidative damage of biomacromolecules. J. Biol. Chem., **269**, 1621-1626.

Zager, R.A. and Burkhart, K.M. (1998): Differential effects of glutathione and cysteine on Fe2+, Fe3+, H2O2 and myoglobin-induced proximal tubular cell attack. Kidney Int., **53**, 1661-1672.

Zhang, Z., Teruya, K., Eto, H. and Shirahata, S. (2011): Fucoidan extract induces apoptosis in MCF-7 cells via a mechanism involving the ROS-dependent JNK activation and mitochondria-mediated pathways. PloS One, **6**, e27441.